

Galaxy Rotation Curves Disfavor Traditional and Self-interacting Dark Matter Halos, Preferring a Disk Component or Einasto Function

Nicolas Loizeau and Glennys R. Farrar Center for Cosmology and Particle Physics, New York University, New York, NY, USA
Received 2021 May 3; revised 2021 August 6; accepted 2021 August 9; published 2021 October 6

Abstract

We use the galaxy rotation curves in the SPARC database to compare nine different dark matter (DM) and modified gravity models on an equal footing, paying special attention to the stellar mass-to-light ratios. We compare three noninteracting DM models: a self-interacting DM model, two hadronically interacting DM models, and three modified Newtonian dynamics type models, modified Newtonian dynamics (MOND), a radial acceleration relation, and a maximal-disk model. The models with DM–gas interactions generate a disky component in the DM, which significantly improves the fits to the rotation curves compared to all other models except an Einasto halo; the MOND-type models give significantly worse fits.

Unified Astronomy Thesaurus concepts: Baryonic dark matter (140); Dark matter (353); Galaxy rotation curves (619); Galaxy dynamics (591); Galaxy physics (612)

1. Introduction

The study of galactic dynamics raised a missing-mass problem (Rubin et al. 1980). Two main models claim to solve it: modified Newtonian dynamics (MOND) and cold dark matter (CDM; Milgrom 1983; Blumenthal et al. 1984). Even though noninteracting CDM models are very successful, they potentially raise new problems, such as the "core-cusp" problem, the explanation of bulgeless galaxies, the missingsatellite problem, and the "too big to fail" problem (Bullock & Boylan-Kolchin 2017). Proposed solutions include self-interacting dark matter (SIDM) and the indirect effects of "gastrophysics": baryon interactions that feed back on the dark matter (DM) via gravity to smooth the cusp (Spergel & Steinhardt 2000; Pontzen & Governato 2012; Ren et al. 2019; Santos-Santos et al. 2020, and many others). Such effects could be enhanced by a DM interaction with baryons. A specific realization of the latter possibility is that the DM particle is an as-yet-undiscovered neutral stable hadron composed of six quarks, *uuddss* (sexaquark; Farrar 2017a, 2018; Farrar et al. 2020). The cross section of such a DM particle with baryons could potentially be large enough that interactions with gas cause the DM to locally take on a similar structure to the gas in the galactic disk (Farrar 2017b). The nature of such a disk would depend on the strength of the coupling, but generically, the DM disk would be thicker than the gas disk, since the DM forming the disk has mostly scattered only once. Therefore, the constraints of Schutz et al. (2018) do not apply.

Our goal here is to compare these different models on an equal footing using the best available rotation curves, those of the Spitzer Photometry and Accurate Rotation Curves (SPARC) database (Lelli et al. 2016). We selected nine models to test: two traditional noninteracting DM halos (Navarro–Frenk–White, NFW, and pseudoisothermal, pIso), an SIDM model (Ren et al. 2019), two models including DM–baryon interactions, MOND, the radial acceleration relation (RAR) ansatz (McGaugh et al. 2016), the maximal-baryon model (Swaters et al. 2012), and, finally, the Einasto functional form, which was found to give the best overall fit to the SPARC rotation curves of the functions explored in the study of Li et al. (2020).

The main limitation in galaxy rotation curve fitting is the uncertainty on the stellar mass-to-light ratios of individual galaxies. In our comparative study, we pay particular attention to the handling of stellar mass-to-light ratios. Previous studies used free or fixed stellar mass-to-light ratios for rotation curve fitting. Using fixed values based on stellar population synthesis models relies too much on the quality of such models, while letting the mass-to-light ratio of individual galaxies be fully free sacrifices constraining power. For example, gas scaling fits resulted in an unphysical stellar mass-to-light ratio distribution ranging between zero and $14 M_{\odot}/L_{\odot}$ (Noordermeer 2006; Swaters et al. 2012), strongly discrepant from population synthesis predictions and observations in the literature. Some more recent work (e.g., Katz et al. 2016) restricts M_{\odot}/L_{\odot} to some range but with a flat prior and quite broad range. Here we constrain the fit such that the distribution of mass-to-light ratios has a physical range, with a mean value and width as determined in Swaters et al. (2014), Schombert & McGaugh (2014), McGaugh & Schombert (2014), Meidt et al. (2014), Lelli et al. (2016), and Schombert et al. (2018).

Our analysis reveals a striking improvement in fit quality for the hadronically interacting DM (HIDM) models, which have a disky DM component reflecting the gas disk (especially the physically based "interaction scaling" model), in comparison to standard alternatives. Therefore, we explore (Section 5) what type of HIDM cross section would be needed to account for the rotation curve results and find that the required cross section can be compatible with DM direct detection limits.

While there is a physical motivation for allowing an HIDM disk, an improved fit with a disk component does not prove that a disk component exists. To see whether a comparable improvement can be achieved with a spherically symmetric halo, we explore alternate functional forms. Li et al. (2020) found that the Einasto function, with one more parameter than traditional CDM halos such as NFW or pIso, gave the best fit to the ensemble of SPARC rotation curves of the functions they considered. We find in our analysis that the Einasto function gives a comparably good fit to the HIDM model. We investigate whether the Einasto fits display any distinctive characteristics, such as occupying some subset of the allowed

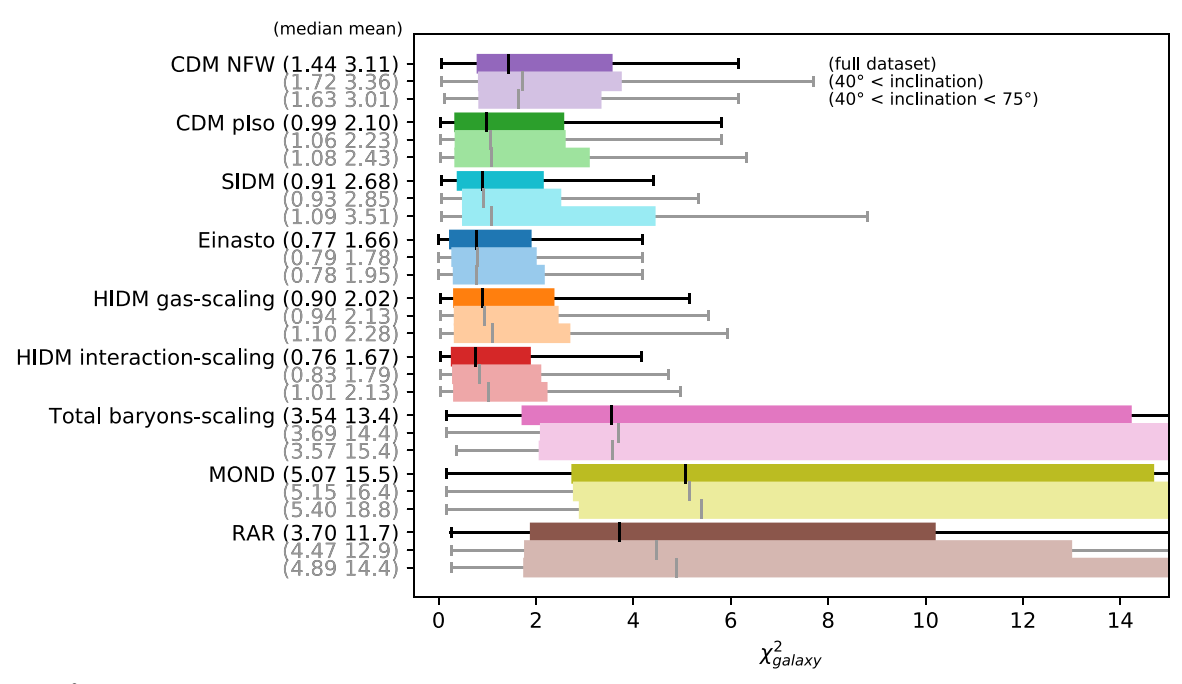


Figure 1. Reduced χ^2 for the models considered, with the median and mean value in parentheses after the model name. The top line for each model corresponds to the entire data set of 121 galaxies, the middle line is for the restricted data set with inclinations greater than 40°, and the bottom line is the restricted data set with inclinations between 40° and 75°. The vertical bar is the median of the individual galaxies' reduced χ^2 , the box contains the values between the first and third quartiles Q1 and Q3, and the right (left) whisker extends to the first χ^2 greater (less than) than Q1 \pm 1.5 (Q3 - Q1). The whiskers on the total baryon scaling, MOND, and RAR models extend to $\chi^2 = 24$, 31, and 21, respectively.

parameter space, but do not uncover any regularities. Future work is needed to understand whether the Einasto form gives a superior fit to simulated galaxies than traditional CDM halo functions, and whether a DM disk may form in simulations with only gravitational DM-baryon interactions. Strategies for observationally distinguishing between spherically symmetric and nonspherical DM distributions are also needed; a new approach is proposed in Loizeau & Farrar (2021).

2. The Data and Models

We use the rotation curves from the SPARC (Lelli et al. 2016) database. The SPARC database is a sample of 175 nearby galaxies representative of the variety of galaxy types. We only use the 121 galaxies with high-quality rotation curves that have 10 or more data points. In Figure 1 and Table 2, we also show the results for a subset of 106 galaxies whose inclinations are greater than 40° and a subset of 71 galaxies whose inclinations are between 40° and 75°.¹ Since removing the more face-on and edge-on galaxies does not change the conclusions within the errors, we use the full data set of 121 galaxies for the rest of the discussion. Additional plots comparing various results using different subsets of galaxies based on inclination and number of points on rotation curves and showing the distribution of galaxies by sampling number can be found in Appendix C.

The SPARC database gives the measured circular velocity of the galaxies as a function of radius, $v_{\rm obs}(r)$. The visible mass components of the galaxies are a gas disk, stellar disk, and stellar bulge, which are also measured. As the total gravitational potential is the sum of the contributions of each mass

component, it is customary to characterize the contribution of each component by v_i^2 such that the sum of all i components satisfies

$$v_{\text{obs}}^2 = \sum_i v_i^2. \tag{1}$$

The v_i are not the velocity of the mass components. They represent the contribution of the mass components to the gravitational potential and hence the total observed velocity $v_{\rm obs}$ via Equation (1).

The SPARC database lists the following quantities as a function of the distance to the center of the galaxies.

- 1. $v_{\rm obs}$: the observed circular velocity.
- 2. σ_{vobs} : the estimated uncertainty on the observed circular velocity.
- 3. $v_{\rm gas}$: the contribution of the gas disk; $v_{\rm gas}$ is derived from the measured H I gas surface densities scaled by a 1.33 factor in order to take into account the presence of helium.
- 4. $v_{\rm disk}$: the contribution of the stellar disk, assuming a stellar mass-to-light ratio of $1 \, M_{\odot}/L_{\odot}$.
- 5. $v_{\rm bulge}$: the contribution of the stellar bulge to the total velocity, assuming a stellar mass-to-light ratio of $1\,M_\odot/L_\odot$.

In converting from the observed distribution of gas and stars to their corresponding v_i^2 quoted in the SPARC database, a thin-disk approximation was used (Lelli et al. 2016).

The models we have considered are detailed in Appendix A. Each model can be written as

$$v_{\text{model},i}^2 = f(v_{*i}^2, v_{\text{gas i}}^2, r_i, \{\text{params}_i\}, \{\text{params}_{\text{model}}\}),$$
 (2)

¹ Edge-on and face-on galaxies labeled by SPARC as high-quality are used in the main data set, because SPARC excludes galaxies whose circular velocity is not well measured from this category.

Table 1
Summary of the Models and Their Free Parameters; for Details, See Appendix A

Model	Global Parameter	Galaxy-dependent Free Parameter	Components	
CDM NFW halo		Υ_*, R_s, ρ_0	Baryons, DM halo	
CDM pIso halo		Υ_*, R_c, ρ_0	Baryons, DM halo	
Einasto		Υ_* , R_s , ρ_0 , α	Baryons, DM halo	
SIDM		$\Upsilon_*, \sigma_{v0}, \rho_0$	Baryons, DM halo	
HIDM-GS		$\Upsilon_*, R_c, \rho_0, \theta$	Baryons, DM halo, DM disk	
HIDM-IS		$\Upsilon_*, R_c, \rho_0, \zeta$	Baryons, DM halo, DM disk	
Total baryon scaling		$\Upsilon_*, heta_b$	Baryons, DM disk	
MOND	a_0	Υ_*	Baryons	
RAR	a_0	Υ_*	Baryons	

Note. The index i on the galaxy-dependent free parameter is dropped for clarity.

where

$$v_{*i}^2 = \Upsilon_{\text{disk},i} v_{\text{disk},i}^2 + \Upsilon_{\text{bulge},i} v_{\text{bulge},i}^2, \tag{3}$$

and f is the model function, i is the index of the galaxy, {params $_i$ } is a set of free parameters that depend on the galaxy, and {params $_{\text{model}}$ } are the model's free parameters. In all models, each galaxy is allowed to have it is own stellar mass-to-light ratio parameter $\overline{\Upsilon}_{i}$ that sets the disk stellar mass-to-light ratios: $\overline{\Upsilon}_{\text{disk},i} = \overline{\Upsilon}_{i}$. In our baseline analysis, we take $\overline{\Upsilon}_{\text{bulge},i} = 1.4 \, \overline{\Upsilon}_{i}$ as suggested by stellar population synthesis models (Schombert & McGaugh 2014). The stellar mass-to-light ratios, $\overline{\Upsilon}_{i}$, are constrained free parameters of the models. We treat them the same way in each model. We verify that allowing $\Upsilon_{\text{bulge},i}$ to be a constrained free parameter does not influence the conclusions (Appendix B); this is not surprising, since very few galaxies have a significant bulge.

Table 1 summarizes the free parameters of the various models.

3. Rotation Curve Fitting and Mass-to-light Ratios

The fits are done by minimizing the reduced χ^2 of a {model, galaxy} pair, defined as

$$\chi_{\text{model},i}^{2} = \frac{1}{n_{i} - \nu_{\text{mod}}} \left[\left(\frac{\Upsilon_{*,i} - \overline{\Upsilon}_{*}}{\sigma_{\Upsilon_{*}}} \right)^{2} + \sum_{j=1}^{n_{i}} \left(\frac{\nu_{\text{obs},i}(r_{j}) - \nu_{\text{model},i}(r_{j})}{\sigma_{\nu_{\text{obs},i}(r_{j})}} \right)^{2} \right].$$
(4)

Here *i* labels the galaxy, *j* is the data point of the rotation curve, n_i is the number of data points for the given galaxy, and ν_{mod} is the number of degrees of freedom per galaxy of the model. We allow $\overline{\Upsilon}_{*,i}$ to vary from galaxy to galaxy, but deviations from the assumed mean value $\overline{\Upsilon}_*$ are penalized by the first term in Equation (4). We only consider galaxies with $n_i \ge 10$, and the median and median value are 19 and 24, respectively. The observational measurement uncertainties used are the uncertainties assigned by SPARC for each data point (Schombert & McGaugh 2014; Lelli et al. 2016).

4. Results of Rotation Curve Fits

Figure 1 gives an overview of the quality of the fits provided by the different models to the magnitude and shape of the rotation curves as a function of radius. The top and bottom lines for each model use the full 121-galaxy and restricted 106-galaxy data set, respectively. The relationship between the fits provided by different models is robust, independent of whether more face-on galaxies are excluded or not.

The reduced χ^2 is distinctly better for the HIDM models than any of the traditional models, including the SIDM and CDM models. Interestingly, the more physical HIDM interaction scaling (HIDM-IS) model gives a better fit than simply scaling to the gas density. Not only is the median χ^2 better than for traditional models, the outliers are also improved. However, the empirical Einasto function does essentially as well as the HIDM-IS model.

Subsets of models with the same number of parameters can be directly compared between themselves, e.g., the CDM and SIDM models, the two HIDM models and the Einasto parameterization, or the MOND and RAR models. A comparison between models with different numbers of parameters is possible using the reduced χ^2 , where the factor $1/(n_{\text{dof},i}=n_i-\nu_{\text{mod}})$ in Equation (4) disadvantages models with more free parameters. There are typically 15–20 data points on the rotation curves of the SPARC galaxies we are fitting, and the minimum number is 10. This means that the differences in the median χ^2 come from the genuinely different radial behaviors possible in the different models.

We can directly verify that the improved fits of the HIDM relative to the CDM and SIDM models is not an artifact of HIDM's having one more parameter by examining how the median χ^2 of the fits change as we increase the minimum number of data points above or below our standard criterion of at least 10. Figure 2 shows the sensitivity to $min(n_{dof})$ for representative models. One sees that, apart from fluctuations, the ranking of models is preserved independent of n_{dof} , except that above $n_{\rm dof,min} \approx 10$ (i.e., for galaxies with more detailed rotation curves), HIDM-IS consistently outperforms Einasto, and SIDM is no better than pIso. The HIDM-IS model is the overall best-fitting model for essentially the entire set of galaxies, although for galaxies with fewer data points, Einasto provides an equally good or sometimes better fit. Thus, the improved χ^2 of the HIDM models indicates a genuinely better description of the shape of the rotation curves than that provided by traditional models.

The significance of the differences between the median χ^2 of the different models can be quantified via a jackknife procedure. We divide the galaxies at random into two halves and calculate their separate median χ^2 ; repeating 1000 times, we recover the ensemble medians and standard deviation (SD)

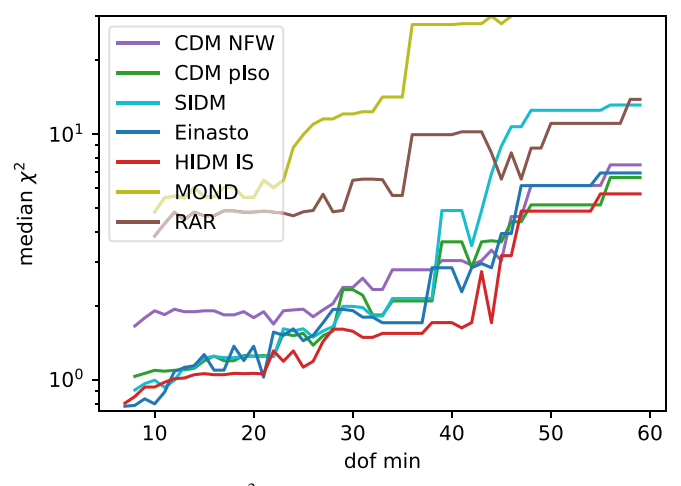


Figure 2. Median reduced χ^2 as a function of the minimum number of degrees of freedom in the fit: $n_{\rm dof} = n_i - \nu_{\rm gal}$. The relative insensitivity to the minimum number of data points required when fitting the rotation curves with the HIDM models shows that the superiority of the HIDM fits is genuine and not an artifact of having one more parameter. It is noteworthy that Einasto is only comparably as good as HIDM-IS for galaxies with small numbers of data points, and HIDM-IS is consistently best for galaxies having more precisely sampled rotation curves. It is unsurprising that when the number of points sampled becomes large, the reduced χ^2 values become systematically worse, because none of these models allow for coherent structures such as seen in the rotation curves of some highly sampled galaxies, e.g., UGC 06787, shown in Appendix D.

of the values for each model. Since these samples have half as many members as the full sample, we estimate a 1σ -like uncertainty as $SD/\sqrt{2}$; the results are shown in Table 2. The HIDM-IS model is 2.7σ better than pIso and 1.7σ better than SIDM, taking σ to be the mean jackknife uncertainty of the pIso and HIDM-IS models, 0.085. The Einasto parameterization offers a similar improvement.

The general properties of the model fits, such as the sensitivity to the mean stellar mass-to-light ratio, and examples of specific galaxies are given in Appendices C and D. Comments on the various models and their fits are given below.

CDM and Einasto Halos

The pIso halo model gives a formally good fit as far as the median $\chi^2=0.99$ goes, with three free parameters per galaxy. With the same number of free parameters, the NFW halo model performs less well, with a median $\chi^2=1.44$ and more outliers with bad χ^2 . It is already well known that rotation curves favor DM cores (Burkert 1995; van den Bosch & Swaters 2001; Gentile et al. 2004). The Einasto halo gives the best fits of its model category to the full data set, with $\chi^2=0.77$. The more flexible functional form and additional α parameter allows the Einasto to reproduce some rotation curve features that cannot be modeled by the two other "simple CDM" models. For example, Einasto fits the galaxies that have a dropping rotation curve at a large radius particularly well (Figure 3). However, it is noteworthy that the benefit of Einasto over pIso is largely restricted to galaxies with relatively few data points, as seen in Figure 2.

SIDM

The SIDM model gives a slightly better median χ^2 than the pIso halo model overall, but for a subset of galaxies, it gives a worse fit. It is systematically worse than pIso for galaxies with many points in their rotation curve, as seen in Figure 2. The

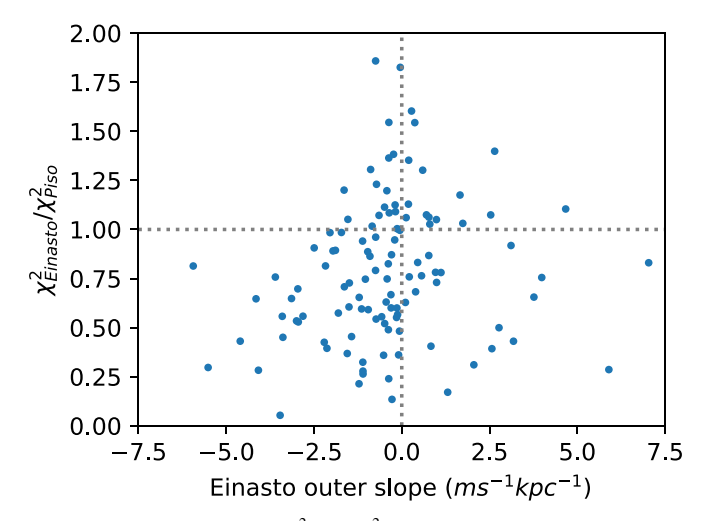


Figure 3. Individual galaxies' $\chi^2_{\rm Einasto}/\chi^2_{\rm plso}$ vs. the outer slope of the Einasto halo contribution to the rotation curve, $dv_{\rm Einasto}/dr$, evaluated at the last data point. The distribution is more populated in the lower left quadrant. These galaxies that have a dropping DM contribution at a large radius are better fit by the Einasto model, while the pIso halo cannot model this particular feature.

success of the SIDM model hinges on the chosen value $\sigma_{\text{SIDM}}/m \approx 3 \text{ cm}^2 \text{ g}^{-1}$, where σ_{SIDM} is the DM self-interaction cross section at the typical relative velocity, and m is the DM mass. Here σ_{SIDM}/m governs the transition radius between the isothermal halo attributed to self-interactions and the effectively noninteracting NFW profile at large radius, with r_1 defined to be the radius at which there would be one interaction in 10 Gyr for the given σ_{SIDM} . For a large enough σ_{SIDM}/m , the SIDM halos are mostly isothermal halos, which give a better fit than pIso. It should be noted that in the majority of the rotation curves, the transition radius r_1 between the isothermal and NFW profiles is larger than the maximum radius for which the rotation curve is measured, so for these galaxies, the SIDM model is equivalent to a pure isothermal halo. In some cases, matching up the NFW halos to the isothermal cores at r_1 produces flat outer rotation curves, and this improves the fit relative to the sharper falloff of the isothermal profile.

We went beyond the analysis reported in Ren et al. (2019) to see if a different value of $\sigma_{\rm SIDM}/m$ can give a better fit. The result of our study is shown in the left panel of Figure 4, from which one sees that the optimal SIDM fit is achieved for 3 cm² g⁻¹, the value chosen by Ren et al. (2019). The fit becomes progressively worse for smaller $\sigma_{\rm SIDM}/m$, and below 1 cm² g⁻¹, it is worse than pure isothermal. For higher cross sections, the fit quality remains roughly constant with increasing $\sigma_{\rm SIDM}/m$. It should be noted that $\sigma_{\rm SIDM}/m > 1$ cm² g⁻¹ may be in tension with limits from the Bullet Cluster (Markevitch et al. 2004).

HIDM

The HIDM-IS model consists of adding a DM disk scaled to the DM-gas interaction density profile. This model gives the overall best rotation curve fits of all of the models in our study. For comparison, we also considered the HIDM gas scaling (HIDM-GS) model, in which the DM disk is simply a rescaled gas disk with the same number of free parameters as HIDM-IS. The HIDM-GS model does not give as good a fit as the physically motivated HIDM-IS model but is better than DM-diskless models (except for Einasto). Thus, the hypothesis that a DM disk forms via interaction with the gas may be valid, at least for a substantial fraction of galaxies. We stress that our current

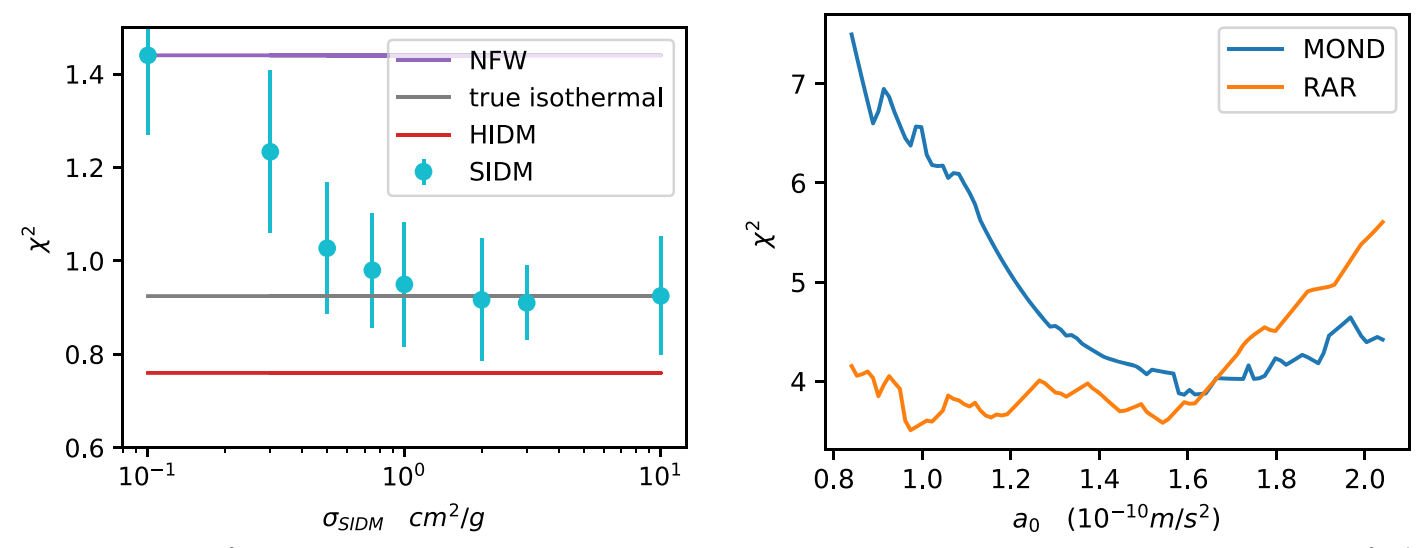


Figure 4. Left: median χ^2 of the SIDM model vs. σ_{SIDM}/m . The error bars correspond to the jackknife uncertainty estimate. When σ_{SIDM}/m is lower than 1 cm² g⁻¹, the isothermal core gets smaller, and the SIDM model provides less benefit relative to NFW. When σ_{SIDM}/m is too low, the SIDM fit is indistinguishable from NFW because the size of the inner core is about one rotation curve data point, so the SIDM model is equivalent to a pure NFW halo. For big cross sections ($\sigma_{\text{SIDM}}/m \gtrsim 10 \text{ cm}^2 \text{ g}^{-1}$), the isothermal core is bigger than the maximum radius for which the rotation curves are measured, and the SIDM model is almost equivalent to a true isothermal halo. Note that there is no noticeable improvement of the SIDM model relative to a pure isothermal halo. Right: median χ^2 of the MOND (blue) and RAR (orange) models vs. acceleration scale a_0 . We adopted $a_0 = 1.2 \cdot 10^{-10}$ m s⁻² as our baseline value; note that this value is acceptable with both variants of MOND, but classic MOND (Equation (A20)) favors $a_0 = 1.6 \cdot 10^{-10}$ m s⁻².

 Table 2

 Median Reduced χ^2 for the Different Models with Jackknife Uncertainty Estimates

NFW	pIso	SIDM	Einasto	HIDM-GS	HIDM-IS	TBS	MOND	RAR
1.44 ± 0.17	0.99 ± 0.08	0.91 ± 0.08	0.77 ± 0.07	0.90 ± 0.10	0.76 ± 0.09	3.54 ± 0.53	5.07 ± 0.71	3.70 ± 0.45
1.63 ± 0.21	1.08 ± 0.15	1.12 ± 0.21	0.78 ± 0.13	1.10 ± 0.14	1.04 ± 0.16	3.81 ± 1.23	5.40 ± 1.32	5.54 ± 1.08
1.89 ± 0.23	1.11 ± 0.16	1.12 ± 0.17	1.14 ± 0.21	1.17 ± 0.17	1.04 ± 0.13	5.11 ± 1.14	6.04 ± 1.30	4.80 ± 0.66

Note. The first line corresponds to the entire data set of galaxies with seven or more points on the rotation curve, the second line corresponds to the restricted data set with inclinations between 40° and 75° , and the third line corresponds to restricting to galaxies with sufficient data points that $N_{\text{dof}} \ge 15$ for the given model.

analysis does not constrain the disk thickness; it approximates the contribution to v^2 as following that of the gas, which is modeled in thin-disk approximation.

We also fitted the rotation curves with an HIDM-IS model but using an SIDM rather than a pIso halo. The median χ^2 does not improve significantly (although the tail with larger χ^2 is reduced); this is compatible with the expectations of the sexaquark DM model, in which the DM self-interactions have been constrained to be too weak to have a significant astrophysical impact (Farrar et al. 2020).

MOND, RAR, and Total Baryon Scaling

To enable maximal performance for the MOND and RAR models, we allowed their parameter a_0 to vary; the median χ^2 values of the corresponding best fits to the data are shown in the right panel of Figure 4. The mean χ^2 values of the MOND and RAR models intersect at $a_0=1.6\cdot 10^{-10}~{\rm m\,s^{-2}}$, around the commonly used acceleration scale $a_0=1.2\cdot 10^{-10}~{\rm m\,s^{-2}}$ (Scarpa 2006). For this value, they give similar quality fits, as shown in Figure 4. The RAR model is still acceptable for lower a_0 , while the original MOND model is still acceptable with an a_0 as high as $2\cdot 10^{-10}~{\rm m\,s^{-2}}$ (Figure 4). The MOND models fail to explain the inner part of the rotation curves of the galaxies with a high central stellar density such as UGC 06787 and F571-8. The

total baryon scaling model yields a better result than MOND, with an additional free parameter per galaxy; however, it is definitely a less effective description than the CDM, SIDM, and HIDM models with DM halos, since its median χ^2 is three to four times higher.

5. Interpreting the Preference for HIDM Models

The most striking result of the analysis presented above is the improvement in the fits to SPARC rotation curves when the DM is not just in a traditional spherically symmetric halo but has a disk component that is scaled to the DM-gas interactions. This does not necessarily mean that DM in galaxies has a disky component, as evidenced by the relatively successful Einasto fits. Even if the DM does have a disky component, that would not prove that it has nongravitational interactions with baryons, since the DM might accrete asymmetrically, on average favoring the same angular momentum axis as the baryonic disk, or it might "relax" to have a disky component aligned

² Note that the best-quality Einasto fits are disproportionately for galaxies with fewer measurements in their rotation curves (Figures 2 and 8); moreover, it has not been established whether the Einasto function gives a good fit to CDM halos in high-resolution simulations, so it is not clear what significance to attach to this.

with the baryonic disk through higher-order gravitational interactions.³

In order to assess whether the improved rotation curve fits provided by the HIDM-IS model could actually be due to DM-baryon interactions, we must investigate whether the values of the HIDM-IS parameter, $\{\zeta_i\}$, are compatible with the bounds on DM-baryon interactions provided by direct detection and other limits. This is the aim of this section.

We can contemplate two extreme possibilities for how robust a DM disk is.

- 1. The DM disk is rather fragile and destroyed in any merger with, say, more than a 1:10 mass ratio.
- The DM disk is generally quite robust and only significantly disturbed in a small fraction of major mergers, e.g., when the angular momentum vectors are highly misaligned.

We can also consider two general scenarios for formation of the DM disk.

- (a) The disk builds up gradually, in situ, due to collisions between DM in the halo and gas in the disk. (In a DM– gas collision, sufficient momentum and energy are typically transferred if the DM and gas particles have comparable masses, so that the postcollision DM phasespace distribution naturally approaches that of the gas; Farrar 2017b). In this scenario, the DM available to build up the DM disk is just the portion of the halo DM that overlaps with the gas disk. This is the basis for the HIDM-IS parameterization as discussed in Appendix A.4.
- (b) The DM-gas interactions contributing to the formation of a DM disk occur not only continuously, as in item (a), but also during passages of individual dwarf galaxies through the galactic plane, as they are gradually stripped of some of their stars, gas, and DM. This process is documented by observed stellar streams such as the Sagittarius stream, PAL-5, and GD-1. To first approximation, when averaged over time, this mechanism would just enhance the ζ value relative to item (a).

It can happen that in some galaxies, item (a) is dominant in determining ζ_i , while in other galaxies, item (b) produces a significant enhancement in ζ_i due to the present-day pIso halo underestimating the time-averaged DM density in the gas disk region.

The upper left panel of Figure 5 displays a histogram of the 121 ζ_i values for the HIDM-IS fit, with the cumulative distribution in the upper right panel. The lower left panel shows the ratio of the mass of the DM disk in the *i*th galaxy relative to the mass of its pIso DM halo versus $\log \zeta_i$. The lower right panel of Figure 5 shows the improvement in χ^2 for the HIDM-IS model relative to the same model with no DM disk (the pIso model).

The majority of galaxies require $\{\zeta_i\}$ in the range $(10^{-8}-10^{-9}){\rm kpc}^3/(M_{\odot}~{\rm km~s}^{-1})^{-1}$ and show significant improvement in the fit to rotation curves due to the DM disk. The DM disks of these galaxies typically carry 1%-10% of the mass of

the pIso halo, with a few galaxies calling for an even greater DM disk fraction (lower left panel of Figure 5). Four galaxies have a more massive DM disk than halo; their rotation curve fits are shown in Figure 17 of the Appendix, making it evident how much better a fit is obtained with the DM disk in these examples. A second population shows negligible improvement in χ^2 from the presence of a disk component and has $\zeta_i \lesssim 10^{-10} \, \mathrm{kpc}^3/(M_\odot \, \mathrm{km \, s^{-1}})^{-1}$. These galaxies can be interpreted as having had a DM disk-busting merger recently enough that they have not yet rebuilt a substantial DM disk.

Galaxies whose DM disks develop through continuous disk growth for some time T_i are the inspiration for the HIDM-IS model, in the approximation that the current gas disk is typical of the average gas disk over time T_i and the circular velocity provides a fair estimate of the DM-gas relative velocity. A range of ζ_i values around the mean would arise due to time variations in individual gas disks, and a population of higher- ζ values could also, in principle, be explained as instances in which a correspondingly higher fraction of the DM came into contact with gas in the disk, as would be the case if entire dwarf galaxies with all of their halo DM passed through the gas disk multiple times before being fully merged into the halo.

From Equation (A14), we have the relationship between ζ_i and the DM–gas cross section and accumulation time T_i in the idealized HIDM-IS model assuming continuous accumulation at the current rate:

$$\zeta_i = \frac{\overline{\sigma_{\rm DM}}}{\overline{m_{\rm gas}}} T_i . \tag{5}$$

In this expression, $\overline{\sigma_{\rm DM}}$ is the abundance-weighted DM–gas cross section, assumed in the present HIDM-IS analysis to be velocity-independent, and $\overline{m_{\rm gas}}$ is the mean mass of the gas particles, which for Galactic abundances is 2.1×10^{-24} g. For a Yukawa interaction (as applicable for sexaquark DM and many models beyond the standard model), DM–nucleus cross sections are velocity-independent except in regions around a resonance point in the Yukawa parameters, where the cross section is $\sim v^{-2}$ down to $v \approx v_{\rm cst}$, below which it is a constant (Xu & Farrar 2021). Using kpc³/(M_{\odot} km s⁻¹) $\approx 10^{26}$ cm² s g⁻¹, we can invert Equation (5) to find

$$\overline{\sigma_{\rm DM}} = 0.6 \; \zeta_{-9} \; T_{10}^{-1} \; 10^{-24} \; {\rm cm^2} \; ,$$
 (6)

where $\zeta_{-9} \equiv \bar{\zeta} \ 10^9 \approx 1$ and $T = 10 \ T_{10}$ Gyr are the central values for the ensemble of galaxies. Since the neglected effects would increase the time-integrated flux, the true cross section needed will be less than this estimate.

If DM-proton or DM-He scattering dominates $\sigma_{\rm DM}$, Equation (6) is (just) compatible with the latest analysis taking into account nonperturbative and finite-size effects (Xu & Farrar 2021) using the robust cosmic microwave background-based analysis of Dvorkin et al. (2014), Gluscevic & Boddy (2018), and Xu et al. (2018). The cosmological structure formation limits are stronger if Ly α and Milky Way satellite limits are valid, but these may be questionable; see Hui et al. (2017). If valid, these stronger limits would exclude $\sigma_p \gtrsim 10^{-27} \, {\rm cm}^2$ for DM mass in the sexaquark range, $\approx 2 \, {\rm GeV}$ (Xu & Farrar 2021). However, even these stronger constraints allow a DM-nucleon Yukawa coupling parameter as large as $\alpha = 0.3$ (Xu & Farrar 2021; Farrar et al. 2020), which could allow DM resonant scattering on some heavier nucleus in the interstellar medium to have such a large cross

Another possibility proposed by Hayashi et al. (2007) based on DM-only simulations, where the inner portions of DM halos often have prolate equipotential surfaces oriented so the long direction is in the plane transverse to the angular momentum (where a baryonic disk would form), is that this nontrivial DM geometry could cause rotation curves interpreted with a spherical halo to appear to have a core while actually having a (triaxial) NFW profile.

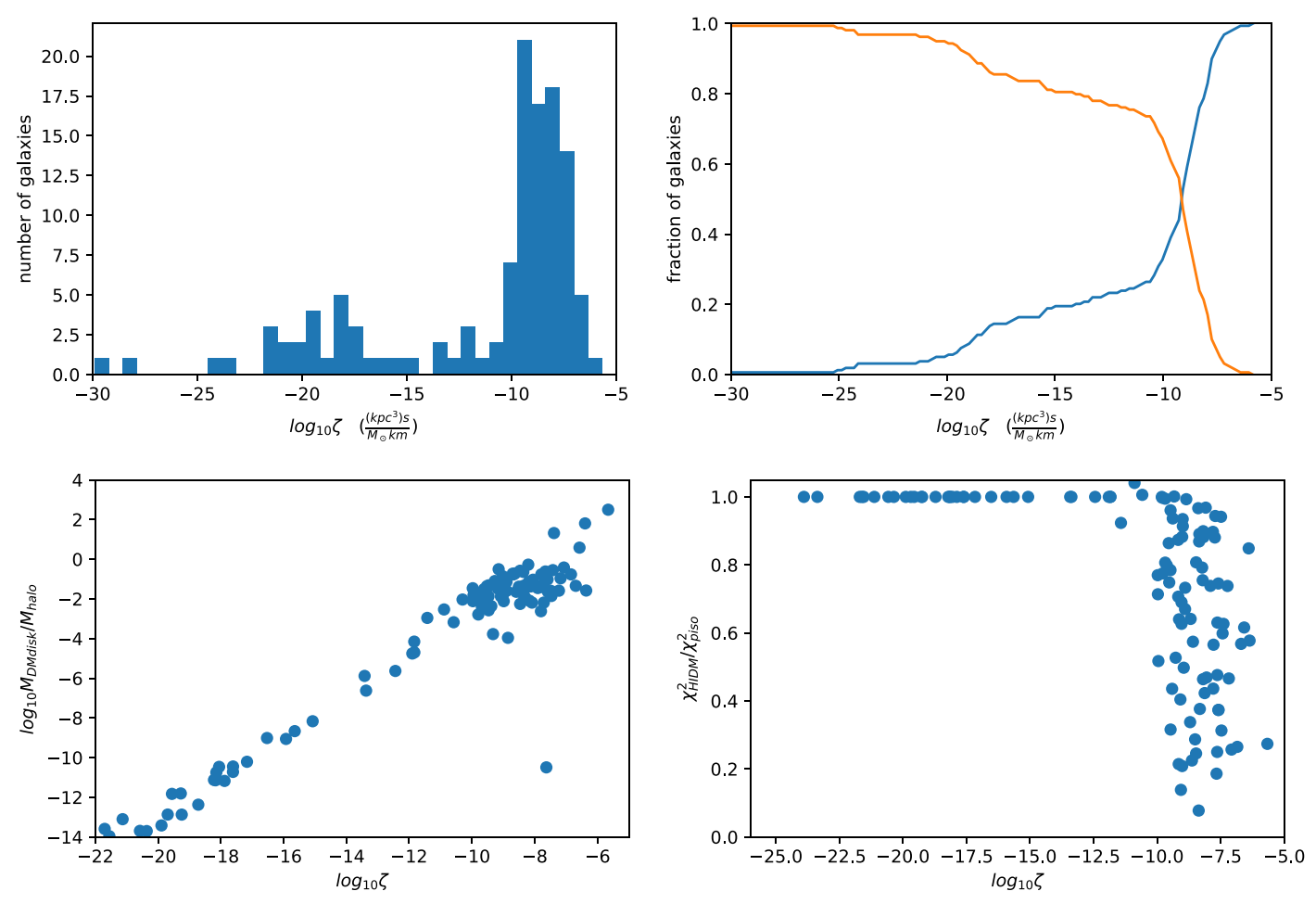


Figure 5. Upper left: distribution of individual galaxies' ζ_i values. Upper right: cumulative distribution of individual galaxies' ζ_i values (blue) and its complement (orange). Lower left: ratio of DM disk to DM halo mass vs. the best-fit $\log_{10} \zeta_i$. Lower right: improvement in the χ^2 for the HIDM-IS model relative to the pIso model as a function of $\log_{10} \zeta_i$; ζ is given in units of $\ker^3 (M_{\odot} \operatorname{km s}^{-1})^{-1}$.

section as to satisfy Equation (6) in spite of a modest fractional abundance. To further test such a scenario requires simulations to determine the true integrated flux of DM on gas, taking into account dwarf galaxies being stripped and assimilated into the galaxy and accounting for the velocity dependence of the dominant DM–nucleus cross section near resonance.

6. Summary and Conclusions

We tested nine different DM and MOND-type models on the rotation curves of 121 galaxies in the SPARC database that have high-quality circular velocity measurements at 10 or more radii, as well as high-quality measurements of the contribution of gas and stars to the rotation curve. We took the stellar mass-to-light ratios of individual galaxies to be fit parameters, constraining the mean value and variance to agree with observations and stellar population synthesis modeling: $\overline{\Upsilon}^* = 0.5 \ M_{\odot}/L_{\odot}$ and $\sigma_{\Upsilon_*} = 0.25 \ \overline{\Upsilon}_*$ (Schombert et al. 2018). Requiring a realistic distribution of Υ^* values had not previously been done.

Figure 1 and Table 2 distill the results. The MOND-type models provide a very much worse description of the ensemble of galaxy rotation curves than the DM models, with a median reduced χ^2 a factor of 3–4 larger. The RAR model is only marginally better than the classic MOND model. The plso DM halos describe the DM mass distributions better than pure NFW

halos, as already known. The SIDM model does slightly better overall than the pIso model for $\sigma/m\gtrsim 3\,\mathrm{cm}^2\,\mathrm{g}^{-1}$ but is not as good as pIso for galaxies with many data points in their rotation curves. For $\sigma/m\lesssim 1\,\mathrm{cm}^2\,\mathrm{g}^{-1}$, the quality of the fit rapidly degenerates, which may be problematic for the SIDM model given the Bullet Cluster and other constraints. The SIDM halo is essentially equivalent to a pure NFW halo for $\sigma/m<0.1\,\mathrm{cm}^2\,\mathrm{g}^{-1}$ and a true isothermal halo for $\sigma/m>10\,\mathrm{cm}^2\,\mathrm{g}^{-1}$; however, for no value of the SIDM cross section does the SIDM model significantly outperform a true isothermal halo in terms of χ^2 per degree of freedom. This challenges the claim that rotation curve fitting favors SIDM above conventional CDM, as suggested by Ren et al. (2019), although it remains an open question whether "gastrophysics" alone can produce an isothermal halo, and SIDM may be helpful for that.

The best-fitting model of the physically motivated ones we investigated is the HIDM-IS model. It postulates that DM interacts with baryons such that DM passing through the gas disk exchanges momentum with gas particles, leading to formation of a DM disk. Our analysis is agnostic about the thickness of the DM disk thus formed, but on physical grounds, it is likely to be thick. In the HIDM-IS model, the surface mass density of the DM disk is proportional to the DM-gas interaction probability—the product of gas and halo DM densities times their relative velocity, approximated by the circular velocity, times cross section. We also considered as a

test a simpler HIDM-GS model in which the DM disk is proportional to the gas disk, with the rescaling factor a fit parameter. If a DM disk is created by interactions with baryons, the HIDM-IS model would be the more realistic description, and indeed, it gives the better fit to the rotation curves. The fact that the fit is better when a more detailed physical modeling of the process is done suggests that DM-gas interactions may be responsible for a disky component of the DM distribution.

As summarized in Table 2, the HIDM-IS model gives a significant improvement of the fit compared to all previously proposed physically motivated models. The reduced χ^2 for the HIDM-IS and Einasto models is 2.7σ better than for the SIDM and 1.7σ better than for the pIso model, although the relative quality of Einasto decreases for galaxies with more points on their rotation curves. We estimated what DM-baryon effective cross section would be needed to account for the HIDM-IS effect in a minimal accumulation scenario and found that even this upper bound on the needed cross section may be compatible with observational limits on DM-baryon scattering.

In most previous studies of rotation curves, the DM distribution has been assumed to be spherical. We have shown that introduction of a (presumably thick) DM disk in addition to a spherical DM halo significantly improves the rotation curve fits in about 80% of the galaxies. An empirical Einasto fitting function gives as good an overall fit as the physically motivated HIDM-IS model on the overall data set consisting of galaxies with at least seven points on their rotation curves, although Einasto does worse for galaxies with better-sampled rotation curves.

Better-measured rotation curves for a larger sample of galaxies and new analysis methods to observationally detect the presence of a thick DM disk or other DM asphericity, e.g., Loizeau & Farrar (2021), are needed. Simulations of galaxy formation including baryonic physics should be analyzed to determine whether DM disks may form by gravitational DM-baryon interactions alone, so that the success of the HIDM-IS model may not imply DM-baryon interactions. If DM disk formation does require HIDM interactions, simulations of galaxy assembly in the presence of HIDM interactions are needed to find the required DM-baryon effective cross section.

We have benefited from discussions with and input from Stacy McGaugh, Marco Muzio, Digvijay Wadekar, and Manoj Kaplinghat and the suggestion of the anonymous referee to investigate a possible inclination-angle dependence of the results. The research of G.R.F. was supported in part by NSF-PHY-2013199.

Appendix A The Models

A.1. CDM: NFW, pIso, and Einasto Halos

Here we model the mass distribution as a baryonic disk surrounded by a spherical DM halo. We consider three halo distributions: an NFW halo (Navarro et al. 1996), a pIso halo (Jimenez et al. 2003), and an Einasto halo. The NFW halo is suggested by pure CDM simulations (Navarro et al. 1997), but the density diverges as r goes to zero (i.e., the distribution is cuspy). The pIso halo appears to be better adapted to describe observed DM cores and has been argued to emerge when feedback is included in the simulations. The Einasto density function was introduced to describe stellar cluster profiles

(Einasto 1965). It was first used to fit CDM halos in dissipationless *n*-body simulations by Navarro et al. (2004) and was recently shown to give a superior empirical description of the SPARC and THINGS rotation curve data (Li et al. 2020; Chemin et al. 2011).

The corresponding halo mass densities are given by

$$\rho_{\text{NFW}}(r) = \frac{\rho_0}{\frac{r}{R_s} \left(1 + \frac{r}{R_s}\right)^2},\tag{A1}$$

$$\rho_{\text{pIso}}(r) = \frac{\rho_0}{(1 + r/R_c)^2},\tag{A2}$$

$$\rho_{Einasto}(r) = \rho_0 \exp\left(-\frac{2}{\alpha} \left[\left(\frac{r}{r_s}\right)^{\alpha} - 1 \right] \right)$$
 (A3)

where ρ_0 , R_s , R_c , r_s and α parameterize the halos. The mass inside a radius r is given by

$$M_{\text{NFW}}(r) = \int_0^r 4\pi r'^2 \rho_{\text{NFW}}(r') dr'$$

$$= 4\pi \rho_0 \left[ln \left(\frac{R_s + r}{R_s} \right) - \frac{r}{R_s + r} \right]$$
(A4)

and

$$M_{\text{Einasto}}(r) = 4\pi \rho_0 R_s^3 e^{\frac{2}{\alpha}} \left(\frac{2}{\alpha}\right)^{-\frac{3}{\alpha}} \times \frac{1}{\alpha} \Gamma\left(\frac{3}{\alpha}, \frac{2}{\alpha} \left(\frac{r}{r_s}\right)^{\alpha}\right), \tag{A5}$$

where Γ is the incomplete gamma function.

The halo is by assumption a spherically symmetric distribution, so the contribution to the rotation curve is given by

$$v_{\text{NFW/Einasto}}^2(r) = G \frac{M_{\text{NFW/Einasto}}(r)}{r}.$$
 (A6)

For the pIso halo, we use (Jimenez et al. 2003)

$$v_{\text{plso}}^2 = 4\pi G \rho_0 R_c^2 \left(1 - \frac{R_c}{r} \tan^{-1} \left(\frac{r}{R_c} \right) \right).$$
 (A7)

Both of these CDM models are described by

$$v_{\text{model}}^2 = v_*^2 + v_{\text{gas}}^2 + v_{\text{halo}}^2$$
, (A8)

and both the NFW and the pIso model have three free parameters per galaxy: Υ_* ; ρ_0 , the characteristic density of the halo; and R_s or R_c , the scale or core radius of the halo.

Figure 6 gives additional information on the Einasto parameters found to give optimal fits to the SPARC data set.

A.2. SIDM

The SIDM has been a popular way to reconcile the smooth cores of galaxies in the face of the cuspy NFW behavior with DM only since the seminal paper of Spergel & Steinhardt (2000). See also Kaplinghat et al. (2014, 2016). Recently, Ren et al. (2019) argued that SIDM provides an excellent fit for galaxy rotation curves. In this section, we compare the quality of such SIDM fits to the other models we consider.

The SIDM self-scattering is most prevalent in the inner part of the halo where the density is high, while it is negligible in the outer part. Hence, following Ren et al. (2019), we model

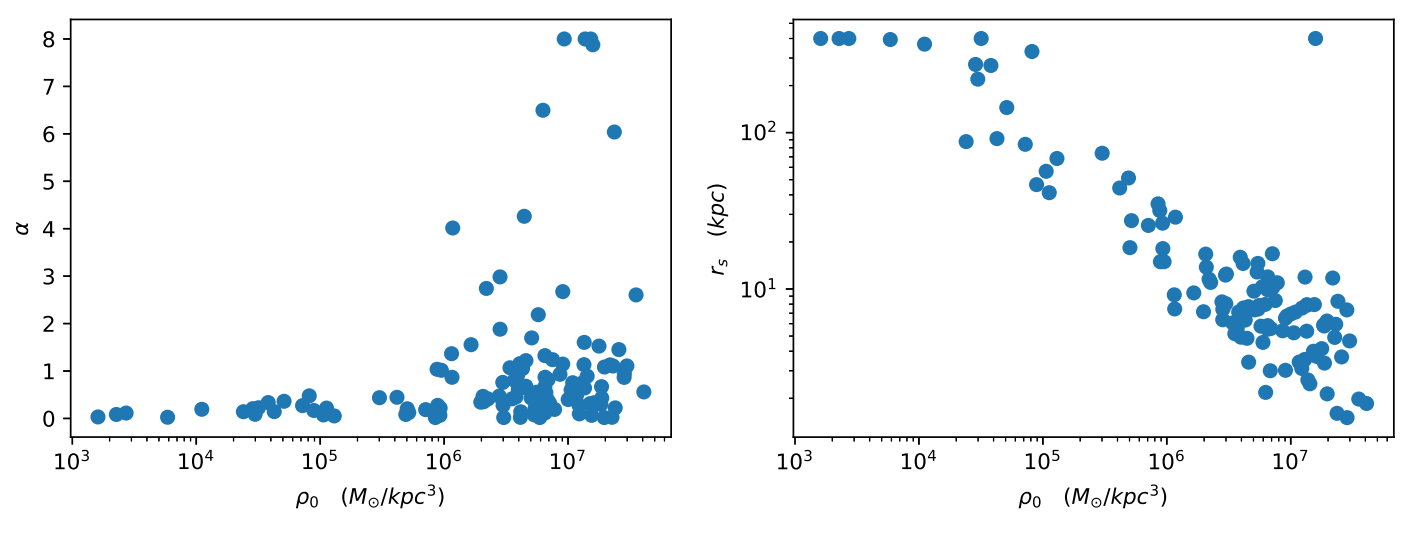


Figure 6. Left: scatter plot of the radial falloff and central density parameters, ρ_0 and α , best fitting the full data set of 121 SPARC galaxies. Right: same as left panel but for the radial scale r_0 and ρ_0 .

SIDM halos by joining an inner isothermal halo with an outer NFW halo at $r = r_1$, interpreted as the characteristic radius of a DM particle scattered only once during the lifetime of the galaxy:

$$\langle \sigma_{\text{SIDM}} v \rangle \rho_{\text{NFW}}(r_1) t_{\text{age}} / m = 1.$$
 (A9)

Here m is the DM particle mass, σ_{SIDM} is the DM self-interaction cross section, v is the DM relative velocity in the halo, t_{age} is the age of the galaxy set to 10 Gyr, and σ_{SIDM}/m is set to $3 \text{ cm}^2 \text{ g}^{-1}$ as in Ren et al. (2019).

We determine the isothermal profile by solving the Poisson equation,

$$\nabla^2 \Phi_{\text{tot}} = 4\pi G (\rho_{\text{iso}} + \rho_{\text{baryons}}), \tag{A10}$$

with $\rho_{\rm iso}=\rho_0 e^{(\Phi(r=0)-\Phi)/\sigma_{\nu 0}^2}$, where $\sigma_{\nu 0}$ is the DM velocity dispersion. Following Ren et al. (2019), we treat the baryon distribution as spherically symmetric for solving Equation (A10). The NFW halo matches to the isothermal halo at r_1 , so that the inner mass and the densities are continuous. Hence, the NFW parameters are fully determined by the isothermal halo parameter, and vice versa. The model has three free parameters per galaxy: Υ_* and the isothermal halo parameters ρ_0 and $\sigma_{\nu 0}$. The self-interaction cross section $\sigma_{\rm SIDM}$ does not appear as a parameter because, as in Ren et al. (2019), we fix $\sigma_{\rm SIDM}/m=3~{\rm cm}^2~{\rm g}^{-1}$. We examined this treatment in the Section 4.

A.3. HIDM-GS

In the case where DM has moderate interactions with baryons, DM that passes through the disk exchanges momentum and energy with gas in the disk, resulting in a component of DM that to some extent follows the gas (Farrar 2017b). This motivates the model discussed in this section. Because simulations with gastrophysics have been shown to give isothermal cores, we adopt pIso to be the functional form of the DM halo in both of our HIDM models (Navarro et al. 1996; Chan et al. 2015). Thus,

$$v_{\text{obs}}^2 = v_*^2 + v_{\text{gas}}^2 + v_{\text{DMdisk}}^2 + v_{\text{pIso}}^2.$$
 (A11)

Assuming that there is a DM component that follows the gas in the disk at the level of their surface mass densities, the relation between these two is $\Sigma_{\mathrm{DMdisk}} = \theta \, \Sigma_{\mathrm{gas}}$, so we have

$$v_{\rm DMdisk}^2 = \theta \ v_{\rm gas}^2. \tag{A12}$$

This model has four free parameters per galaxy: Υ_* , the gas-to-DM scale factor θ , and the parameters of the DM isothermal halo, ρ_0 and R_s . We emphasize that the actual DM "disk" represented in this analysis may be much thicker than the gas disk.

A.4. HIDM-IS

This is a more physical version of the previous HIDM model, in which we account for the fact that the DM accumulates where the density of gas–DM interactions is high. If DM and gas particles have similar mass, the exchange of momentum and energy between the DM and gas ejects gas into the halo and leaves the DM in a more disklike configuration (Farrar 2017b; Wadekar & Farrar 2021). The DM also interacts with the gas in the hot gaseous halo, but that gas has a similar velocity dispersion as the halo DM, so such DM–gas scatterings do not modify the halo DM distribution very significantly. The DM in the disk thus scales in proportion to the interaction rate per unit volume Γ (r) between the gas particles in the gas disk and the DM particles in the DM halo:

$$\Gamma(\mathbf{r}) = n_{\text{halo}}(\mathbf{r}) \, n_{\text{gas}}(\mathbf{r}) \, \sigma_{\text{DM-gas}} \, v_{\text{rel}}(\mathbf{r}) \,. \tag{A13}$$

SPARC assumes a thin disk for the contribution of stellar and gas components, and we adopt the same for the scattered DM. In this approximation, the scattered DM particles produce a DM disk whose local surface number density profile is obtained by integrating Equation (A13) over z and the time T_i that the DM disk has been accumulating. Making the simplifying assumption that the present gas distribution and DM halo density in the gas disk region are representative of their values over time, T_i , gives the DM disk surface mass

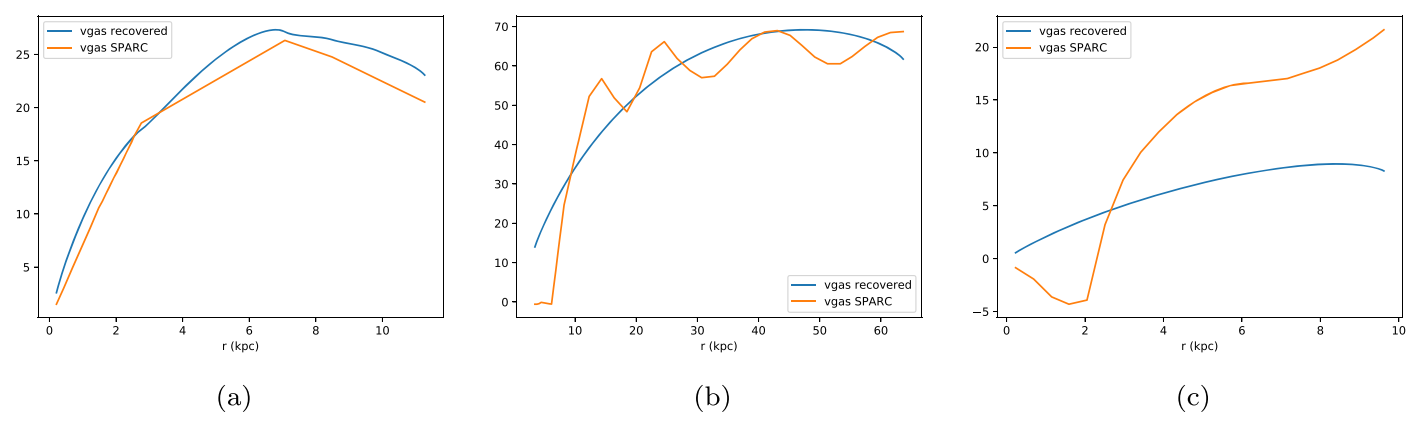


Figure 7. Three representative examples illustrating the fidelity of the procedure used to determine $\Sigma_{\rm gas}$ by fitting $v_{\rm gas}$ with a radially exponential disk $\Sigma_{\rm gas}(r) = \Sigma_0 e^{-r/r_0}$ (Kalberla & Kerp 2009), comparing input and recovered $v_{\rm gas}^2$.

density

$$\Sigma_{\rm DM}(r) = m_{\rm DM} T_i \left(\frac{\rho_{\rm halo}(r)}{m_{\rm DM}} \right) \left(\frac{\Sigma_{\rm gas}(r)}{m_{\rm gas}} \right)$$

$$\sigma_{\rm DM-gas} v_{\rm rel}(r)$$

$$\equiv \zeta_i \rho_{\rm halo,i}(r) v_{\rm obs,i}(r) \Sigma_{\rm gas}(r) . \tag{A14}$$

In the last line, we approximated $v_{\rm rel}(r)$ by the observed circular velocity at radius r and took $\sigma_{\rm DM-gas}$ to be velocity-independent.

Equation (A14) defines the HIDM-IS model with ζ_i as the fitting parameter governing the DM disk. In Section 5, we examine the relationship between the distribution of ζ_i from the fits to this model and the DM-gas cross section, but here we treat the problem empirically with

$$v_{\text{model}}^2 = v_*^2 + v_{\text{gas}}^2 + v_{\text{DMdisk}}^2 + v_{\text{pIso}}^2,$$
 (A15)

where, following Lelli et al.'s (2016) treatment of the gas disk, v_{DMdisk} is derived from Σ_{DMdisk} by using Casertano's method, which is a way to solve Newton's equations for a mass disk (Casertano 1983).

The quantities required to calculate Σ_{DMdisk} are ρ_{pIso} , v_{obs} , and Σ_{gas} ; ρ_{pIso} is determined by the fit, while v_{obs} and Σ_{gas} are observed data. However, we do not have systematic access to the radial surface gas densities of the SPARC data set. In order to compensate for this lack of underlying data, we recover Σ_{gas} by fitting v_{gas} with a radially exponential disk, $\Sigma_{\mathrm{gas}}(r) = \Sigma_0 e^{-r/r_0}$ (Kalberla & Kerp 2009). A few examples of the fidelity of this procedure are given in Figure 7, where we see that the recovered v_{gas}^2 generally agrees to \approx 20%, although small-scale structure is lost. Hopefully, the underlying Σ_{gas} data will become publicly available in the future.

This model has four free parameters per galaxy: Υ_* ; ζ , the DM disk interaction scaling factor; and the parameters of the halo ρ_0 and R_c .

A.5. Total Baryon Scaling

Swaters et al. (2012) fit a set of rotation curves with the model

$$v_{\text{obs},i}^2 = \Upsilon_{\text{disk},i} v_{\text{disk},i}^2 + \Upsilon_{\text{bulge},i} v_{\text{bulge},i}^2 + \eta_i v_{\text{gas},i}^2.$$
 (A16)

Here $\Upsilon_{\text{disk},i}$ $\Upsilon_{\text{bulge},i}$, and η_i are unconstrained free parameters. The resultant fits work well for the majority of the galaxies in their data set. They argued that this means that DM could follow the baryons in those galaxies and an extended halo is not needed

(if the fit parameters $\Upsilon_{\text{disk},i}$, $\Upsilon_{\text{bulge},i}$, and η_i are physically reasonable). However, this fit does not work for a small subset of galaxies. A possible hypothesis to account for that is that those galaxies are recent mergers and the DM is located primarily in a halo rather than following the gas in the disk.

To quantitatively compare the Swaters et al. (2012) model with other models, we study a similar model that scales the total baryon density (bulge, stellar disk, and gas) with a single overall scaling factor θ_b . Effectively, this assumes that there exists a DM component that exactly follows the baryons in the galaxy. (This total-baryons-scaling model could also arise in an extreme case of hadronically interacting DM where the DM initially in a halo would relax to follow the baryonic distribution, including baryons in stars which themselves formed from gas; Farrar 2017b). The relation between the DM and stellar and gas surface mass densities is then $\Sigma_{\rm DMdisk} = \theta_b(\Sigma_* + \Sigma_{\rm gas})$. As v^2 is proportional to the gravitational potential, scaling the densities is equivalent to scaling v^2 . Hence,

$$v_{\text{obs}}^2 = v_*^2 + v_{\text{gas}}^2 + v_{\text{DMdisk}}^2,$$
 (A17)

with

$$v_{\text{DMdisk}}^2 = \theta_b(v_*^2 + v_{\text{gas}}^2).$$
 (A18)

This model has two free parameters per galaxy, θ_b and Υ_* , entering through ν_* .

A.6. MOND and RAR

The acceleration a in the MOND theory is related to the Newtonian acceleration a_N by a new fundamental parameter a_0 and an interpolation function μ (Scarpa 2006),

$$\frac{a_N}{a} = \mu \left(\frac{a}{a_0}\right),\tag{A19}$$

where $\mu(x) = \frac{x}{1 + x^2}$. Solving for a gives

$$a = a_N \sqrt{\frac{1}{2} + \frac{1}{2} \sqrt{1 + \left(\frac{2a_0}{a_N}\right)^2}}$$
 (A20)

Thus, the contribution to the rotation curve is

$$v_{\text{MOND}}^2 = \frac{v_N^2}{r} \sqrt{\frac{1}{2} + \frac{1}{2} \sqrt{1 + \left(\frac{2a_0 r}{v_N^2}\right)^2}},$$
 (A21)

where

$$v_N^2 = v_{\text{gas}}^2 + v_*^2. \tag{A22}$$

Here a_0 is usually set as $1.2 \cdot 10^{-10}$ m s⁻² (Scarpa 2006).

In McGaugh et al. (2016), the existence of an RAR is shown, and the observed acceleration is related to the baryonic acceleration by

$$a = a_N (1 - e^{-\sqrt{a_N/a_0}})^{-1}.$$
 (A23)

This equation can be considered as a new empirical interpolation function that well describes the data.

We fit both the classic MOND and RAR models to the SPARC rotation curves, first for the standard $a_0 = 1.2 \cdot 10^{-10} \,\mathrm{m\,s}^{-2}$ and then for different a_0 values. For convenience, we call Equation (A20) MOND and Equation (A23) RAR; Υ_* is the only free parameter for each galaxy.

Appendix B Stellar Mass-to-light Ratios

The determination of the stellar mass-to-light ratio of a particular galaxy, $\Upsilon_{*,i}$, is a critical step in rotation curve fitting. The standard approach in previous works has been either to leave $\Upsilon_{*,i}$ as a free parameter of the fit for each galaxy, leading to unphysical resultant distributions of $\Upsilon_{*,i}$ or to fix it based on stellar population synthesis models (e.g., Chemin et al. 2011). In this work, we allow $\overline{\Upsilon}_{*,i}$ to vary from galaxy to galaxy, but we penalize deviations from the assumed mean value $\overline{\Upsilon}_*$ by adding a term to the χ^2 in Equation (4). Upper bounds on Υ_* can be derived from the "maximum stellar disk" fit, where one tries to maximize the contribution of the stars to the rotation curve. The mean maximummass-to-light ratio for SPARC $\Upsilon_*^{max} \approx 0.7 M_{\odot}/L_{\odot}$ (Lelli et al. 2016). (Mass-to-light ratios for SPARC galaxies are quoted at 3.6 μ m.) This is substantially higher than the estimated stellar mass-to-light ratio reported in the DiskMass Survey, which gives $\overline{\Upsilon}_* \approx 0.2 M_{\odot}/L_{\odot}$ (Swaters et al. 2014). Stellar population synthesis models report mean values between 0.4 and $0.6 M_{\odot}/L_{\odot}$ (Schombert & McGaugh 2014; McGaugh & Schombert 2014; Meidt et al. 2014). Here we assume that the mean stellar mass-to-light ratio of the SPARC galaxies is $\overline{\Upsilon}_* = 0.5 M_{\odot}/L_{\odot}$, as suggested by Schombert et al. (2018) using data from the main-sequence (stellar mass versus stellar formation rate) and stellar population models. We take $\sigma_{\Upsilon_*} = 0.25 \, \overline{\Upsilon}_*$ from Schombert et al. (2018). For the galaxies that have a bulge, we set $\Upsilon_{\text{bulge}} = 1.4 \Upsilon_{*}$, as suggested by stellar population synthesis models.

Each model fit returns the stellar mass-to-light ratio $\Upsilon_{*,i}$ for each galaxy; the distribution of $\Upsilon_{*,i}$ values is shown in the right panel of Figure 8. The performance in terms of the χ^2 of the tested models is reflected in the distribution of mass-to-light ratios. The DM model fits have a mass-to-light ratio distribution peaked at around 0.5, the assumed average value based on stellar population synthesis models. However, MOND predicts a maximum of the Υ_* distribution around 0.7, significantly larger than inferred from stellar population synthesis modeling (McGaugh & Schombert 2014; Meidt et al. 2014; Schombert & McGaugh 2014).

We adopted $\overline{\Upsilon}_*=0.5$ as the mean value for the study, but to check the sensitivity of the conclusions to this chosen value, we redid the analysis for a range of mean mass-to-light ratios between 0.1 and 1. How the overall quality of the rotation curve fitting depends on $\overline{\Upsilon}_*$ is shown in the right panel of Figure 8 for illustrative cases. One sees that the HIDM models' quality of fit is insensitive to the assumed mean $\overline{\Upsilon}_*$, below ≈ 0.6 , while the CDM models have a stronger preference for some particular $\overline{\Upsilon}_*$. We also find that treating Υ_{bulge} as a constrained free parameter with mean $1.4\overline{\Upsilon}_*$ and spread $0.25\overline{\Upsilon}_*$ does not significantly impact our results. For example, free (fixed) Υ_{bulge} gives $\chi^2_{\text{NFW}}=1.44(1.40)$ and $\chi^2_{\text{pIso}}=0.98(0.99)$. Note that 24% of the galaxies in the data set have a bulge.

Li et al. (2020) did Markov Chain Monte Carlo fitting allowing the galaxy distances and inclinations to vary from the tabulated SPARC values. We decided not to do this because we do not have access to the underlying data needed for a careful analysis; a change in inclination leads to a simple rescaling of $v_{\rm obs}$ but would have nontrivial effects on the inferred v_{gas} and v_* . Nor can we make use of the Li et al. (2020) values, since they were optimized under the assumption of specific DM models, and we have different models. We could consider optimizing the distance independently for each model. Both methods are in good agreement, since we recover $\chi^2_{\rm Einasto} < \chi^2_{\rm plso} < \chi^2_{\rm NFW}$ as in Li et al. (2020), where, for example, 88% of the plso fits have $\left|\frac{D-D_{\text{SPARC}}}{D}\right|$ and 92% have $\left|\frac{\sin(i)-\sin(i_{\text{SPARC}})}{D}\right|$, with D the fit distance, $\sin(i_{\text{SPARC}})$ D_{SPARC} the tabulated distance, i the fit inclination, and i_{SPARC} the tabulated inclination. These inclination and distance adjustments lead to changes in $v_{\rm obs}$ that are small compared to the error $dv_{\rm obs}$ given in SPARC.

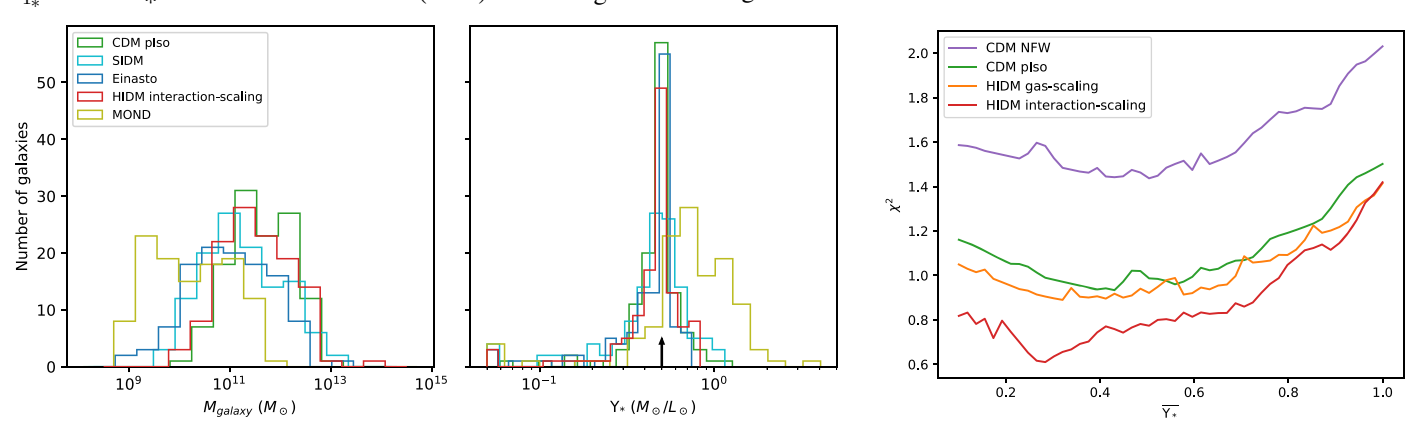


Figure 8. Left: histogram of the galaxy masses according to representative models. Middle: histogram of the stellar mass-to-light ratios derived from the different models. The arrow represents $\Upsilon_* = 0.5$, the assumed mean value. Right: median χ^2_{dof} vs. assumed mean mass-to-light ratio in the fitting. Here $\overline{\Upsilon}_* = 0.5$ is compatible with all of the halo models, in agreement with the Schombert et al. (2018) estimations.

Appendix C General Properties of the Model Fits

The fits enable us to estimate the total mass of each of the galaxies in the sample using the inferred amount of DM. The left panel of Figure 8 shows the resultant distribution of total

SMHR ranges from 1% to 2.5% for redshifts 2 < z < 5 (Durkalec et al. 2015).

We also display in Figure 10 some facets of the inclinationangle and minimum- n_{dof} dependence of the results, concentrating on HIDM-IS and Einasto, the two most successful models.

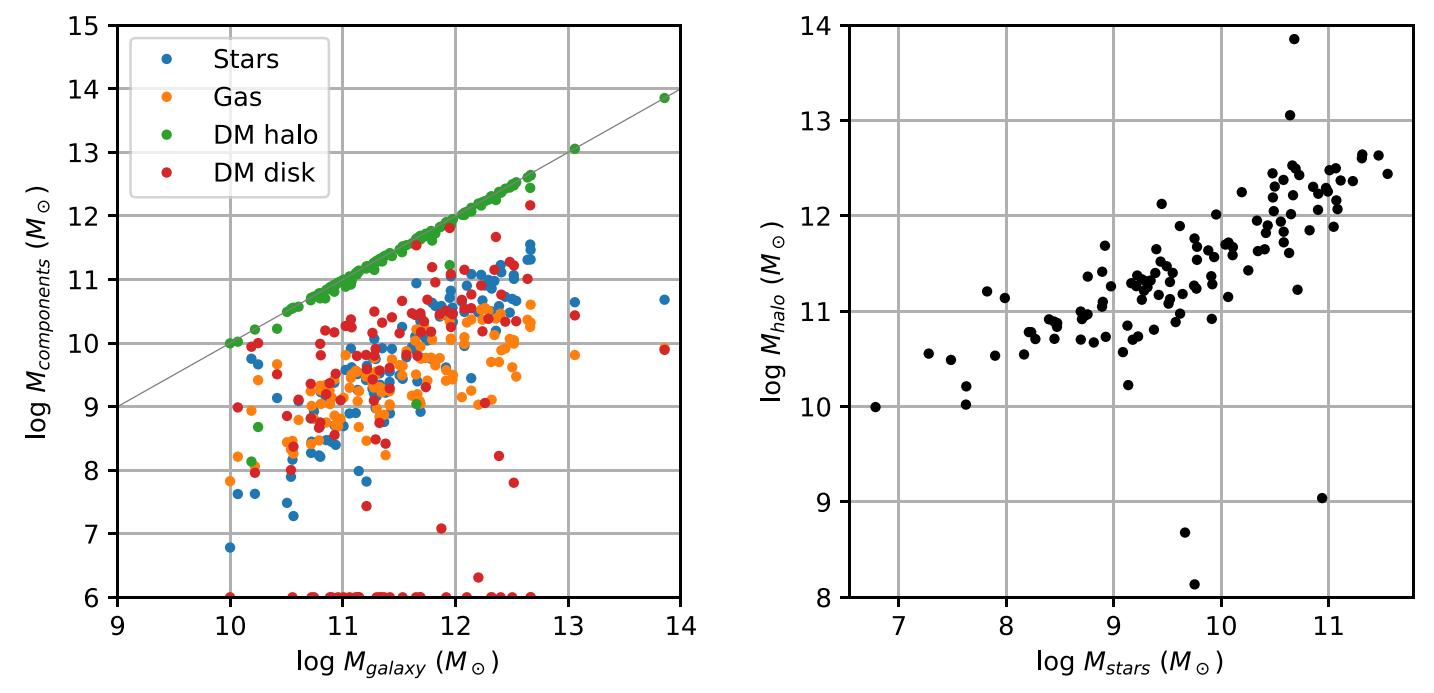


Figure 9. Left: mass of the four components of the HIDM-IS model vs. the total mass of the galaxies. One galaxy is represented by four points. Right: SMHR for the HIDM-IS model.

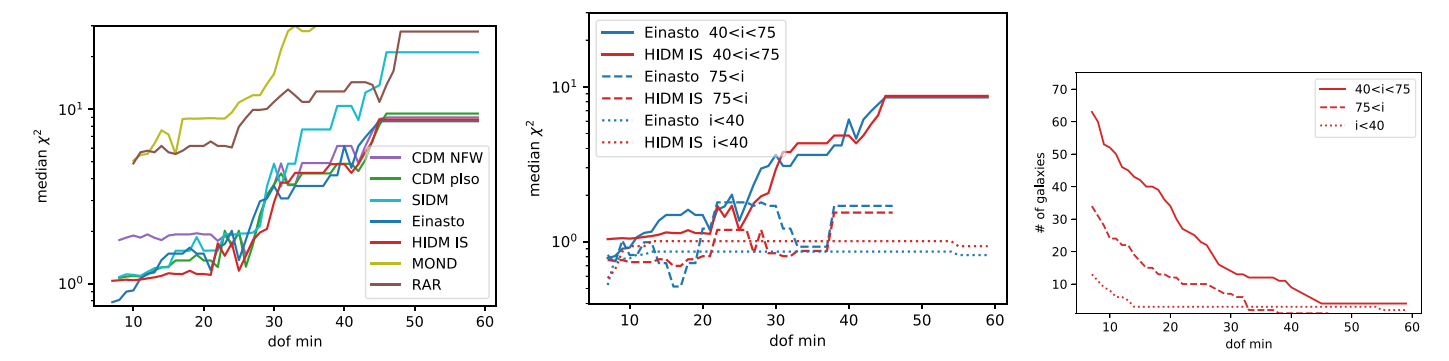


Figure 10. Left: median reduced χ^2 as a function of the minimum number of degrees of freedom in the fit: $n_{\text{dof}} = n_i - \nu_{\text{gal}}$ for the restricted data set with inclinations between 40° and 75°. Middle: same as left panel but for the Einasto and HIDM-IS models, separated by inclination-angle region. Right: number of galaxies in the three inclination-angle bins vs. $n_{\text{dof,min}}$.

galaxy masses for each of the models. Figure 9 displays some important inferred physical features of galaxies for the overall best-fitting model, HIDM-IS. The plots for the HIDM-GS model are similar. The left panel of Figure 9 shows how the total mass of each galaxy is distributed between the stars, the gas, and the two components of the DM. The distribution of the masses of the DM disks is similar to the distribution of the masses of the gas disks, with a median ratio of 2.0. The right panel of Figure 9 shows the correlation between stellar and halo mass. According to the HIDM models, the median stellar mass—to—halo mass ratio (SMHR) is 1.8%. This value is consistent with estimations from the VIMOS Ultra Deep Survey, which finds that the

Appendix D Specific Example Galaxies

To enable the reader to appreciate the successes and inadequacies of the different models for explaining the diversity of rotation curves, we show the rotation curve data for seven illustrative galaxies along with the different models' best fits. These seven galaxies provide a good sample of the variety of fits from among the galaxies in the SPARC database whose rotation curves do not lack data near the galactic center. Figure 11 allows all of the model predictions to be seen together for each of the seven galaxies. Figures 12–16 give a more detailed view of how the different models achieve their

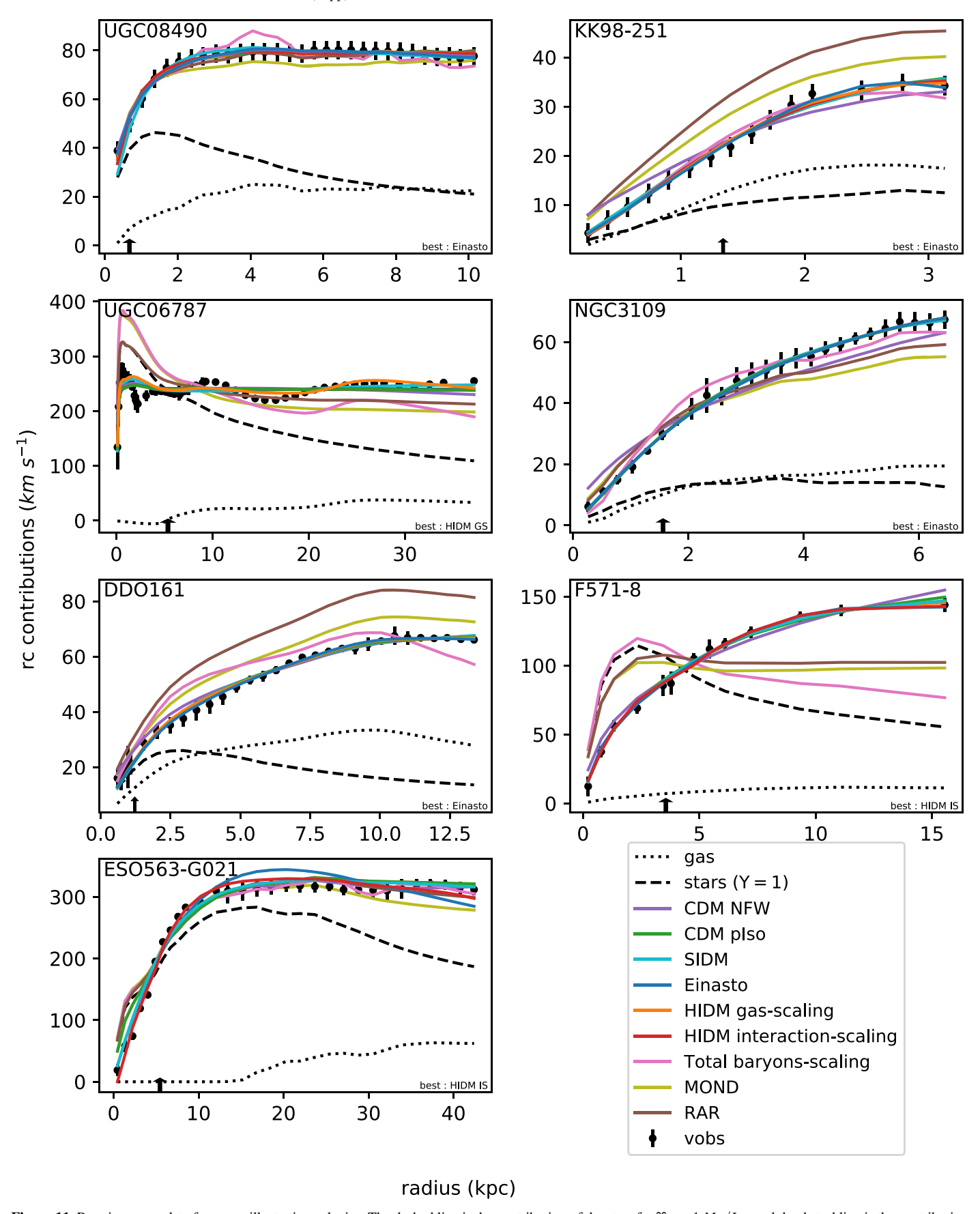


Figure 11. Rotation curve data for seven illustrative galaxies. The dashed line is the contribution of the stars for $\Upsilon_* = 1 M_{\odot}/L_{\odot}$, and the dotted line is the contribution of the gas disk. Colored lines are the best-fit rotation curves for the eight models. The black arrow is the disk scale length (Lelli et al. 2016).

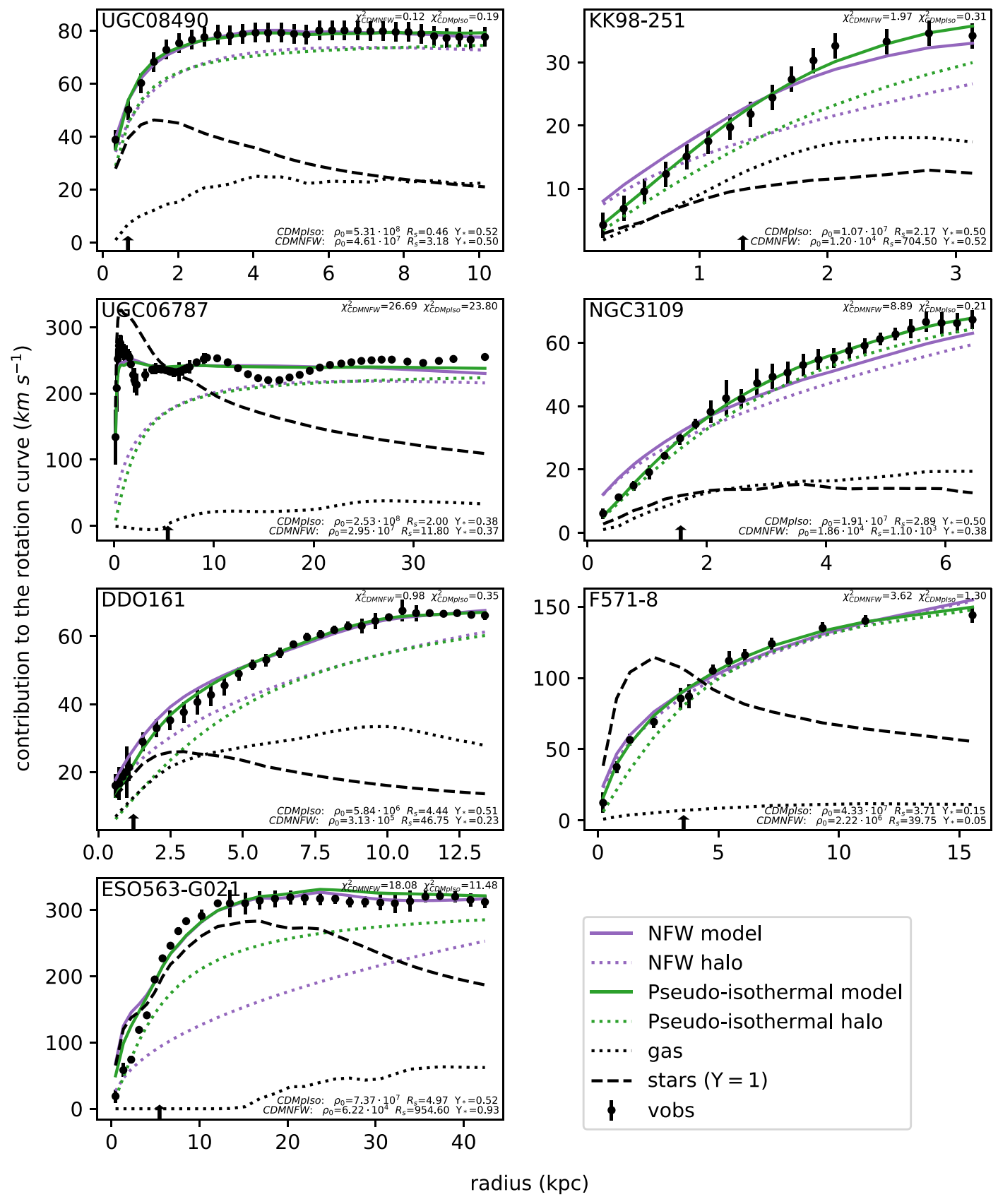


Figure 12. Rotation curve fits of the CDM halo models. The solid lines "NFW model" and "Pseudo-isothermal model" are the total model velocity derived from the fits. The dotted lines "NFW halo" and "Pseudo-isothermal halo" are the contribution of the halo to the total velocity.

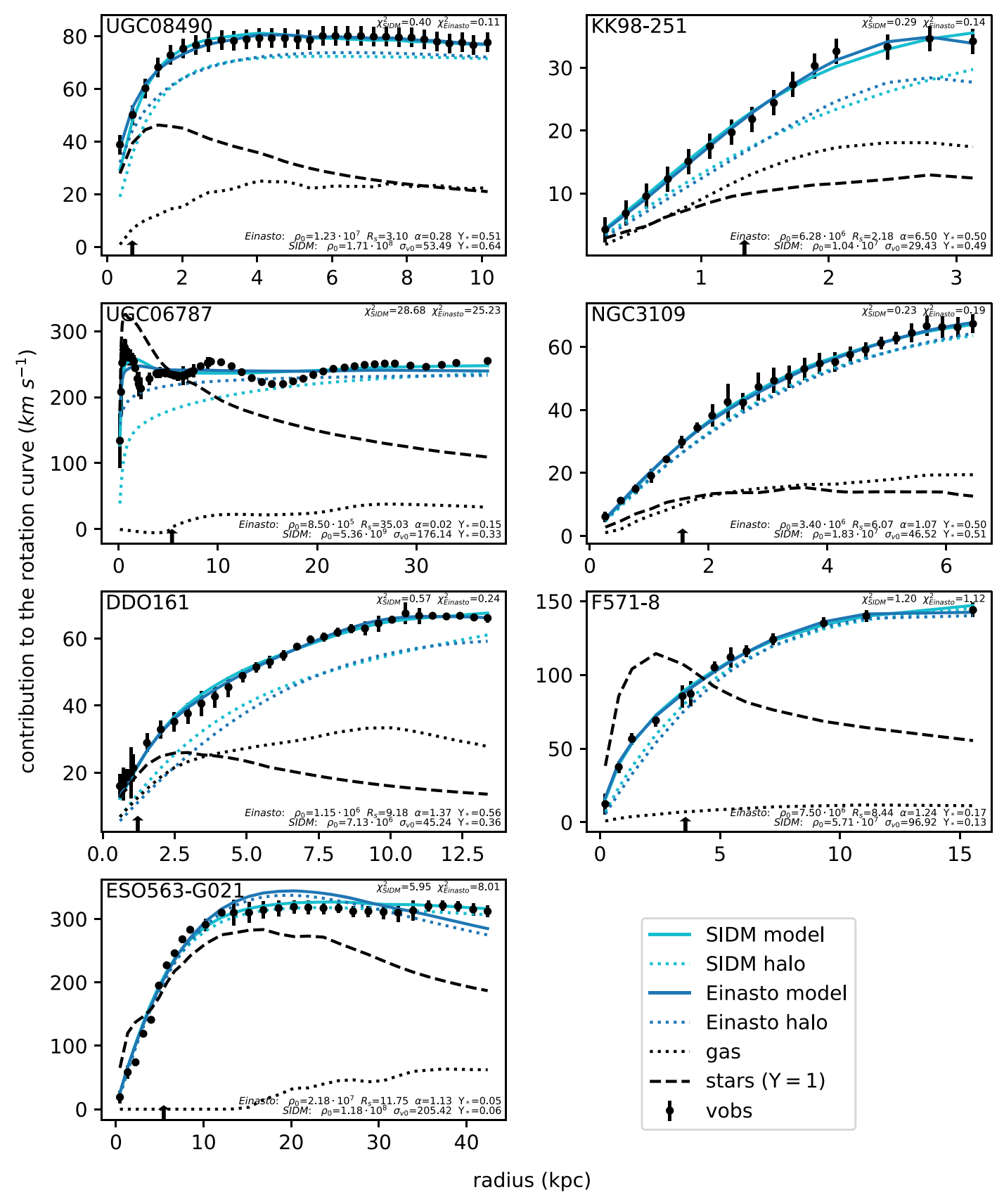


Figure 13. Rotation curve fits of the SIDM and Einasto models. The solid lines "SIDM model" and "Einasto model" are the total model velocity derived from the fits. The dotted lines "SIDM halo" and "Einasto halo" are the contribution of the halo to the total velocity.

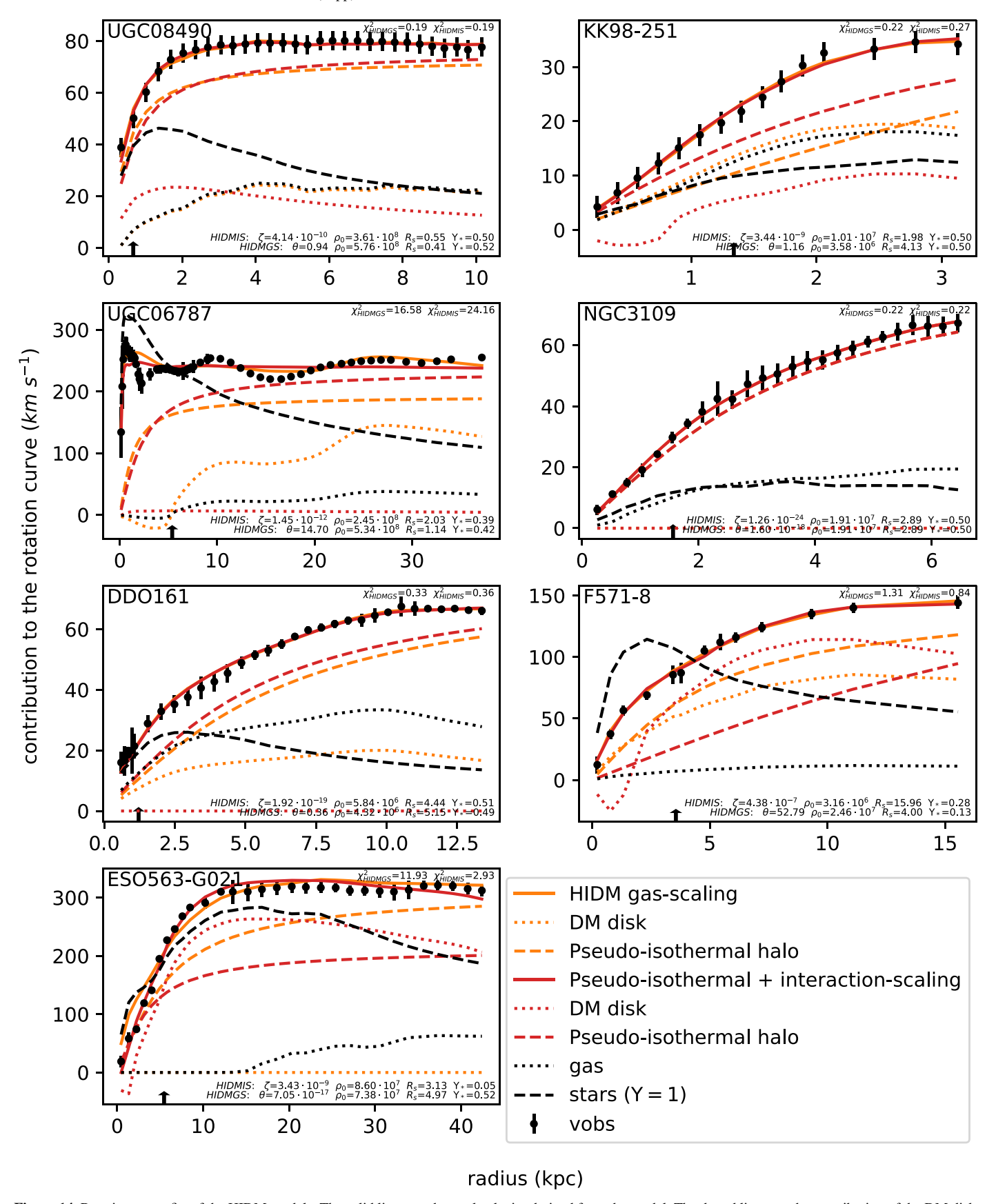


Figure 14. Rotation curve fits of the HIDM models. The solid lines are the total velocity derived from the model. The dotted lines are the contribution of the DM disks to the total velocity. The dashed line is the contribution of the halos to the total velocity.

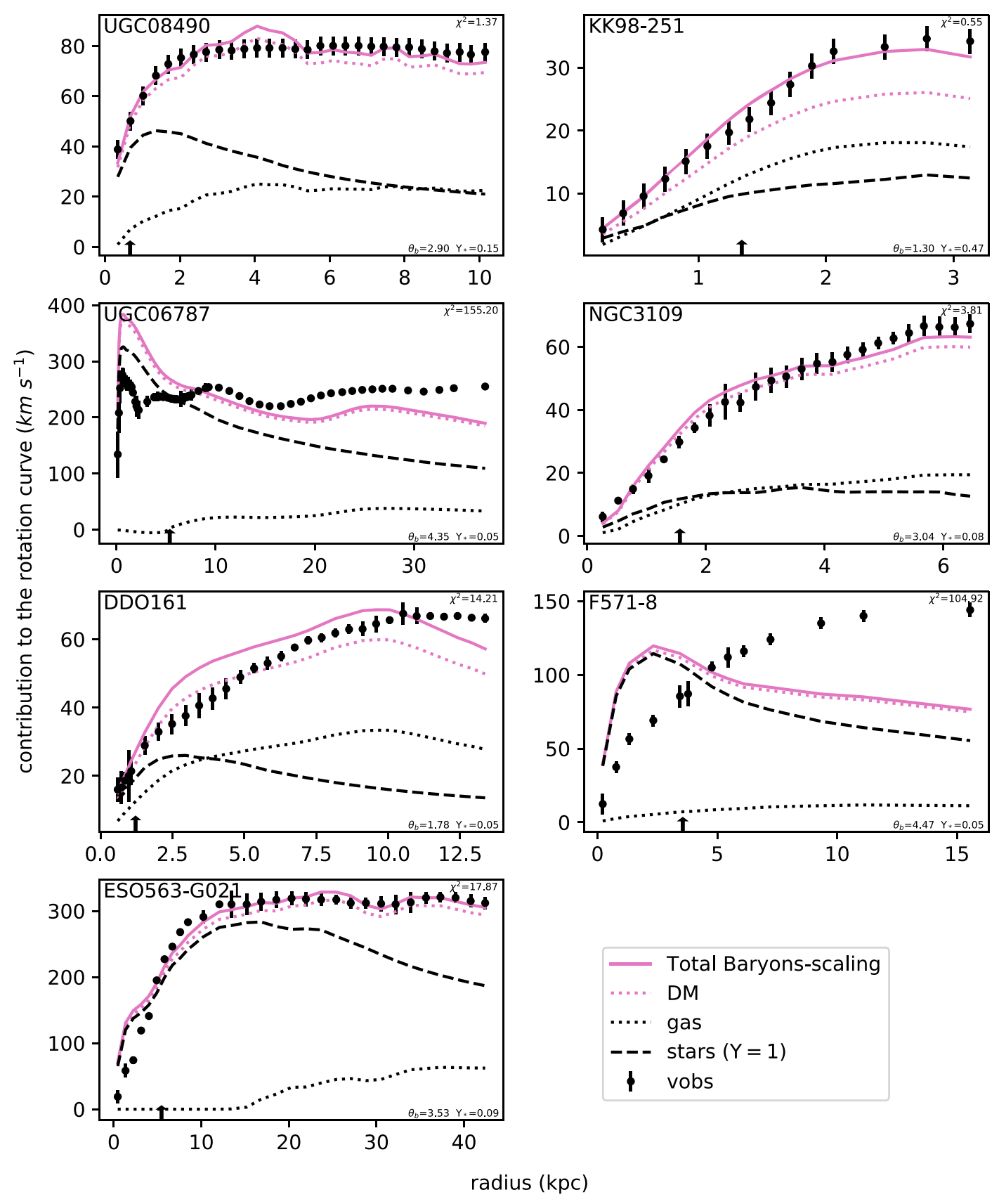


Figure 15. Rotation curve fits of the total baryon scaling models. The magenta solid line is the total velocity derived from the baryon scaling model. The magenta dotted line is the contribution of the DM disk component to the total velocity.

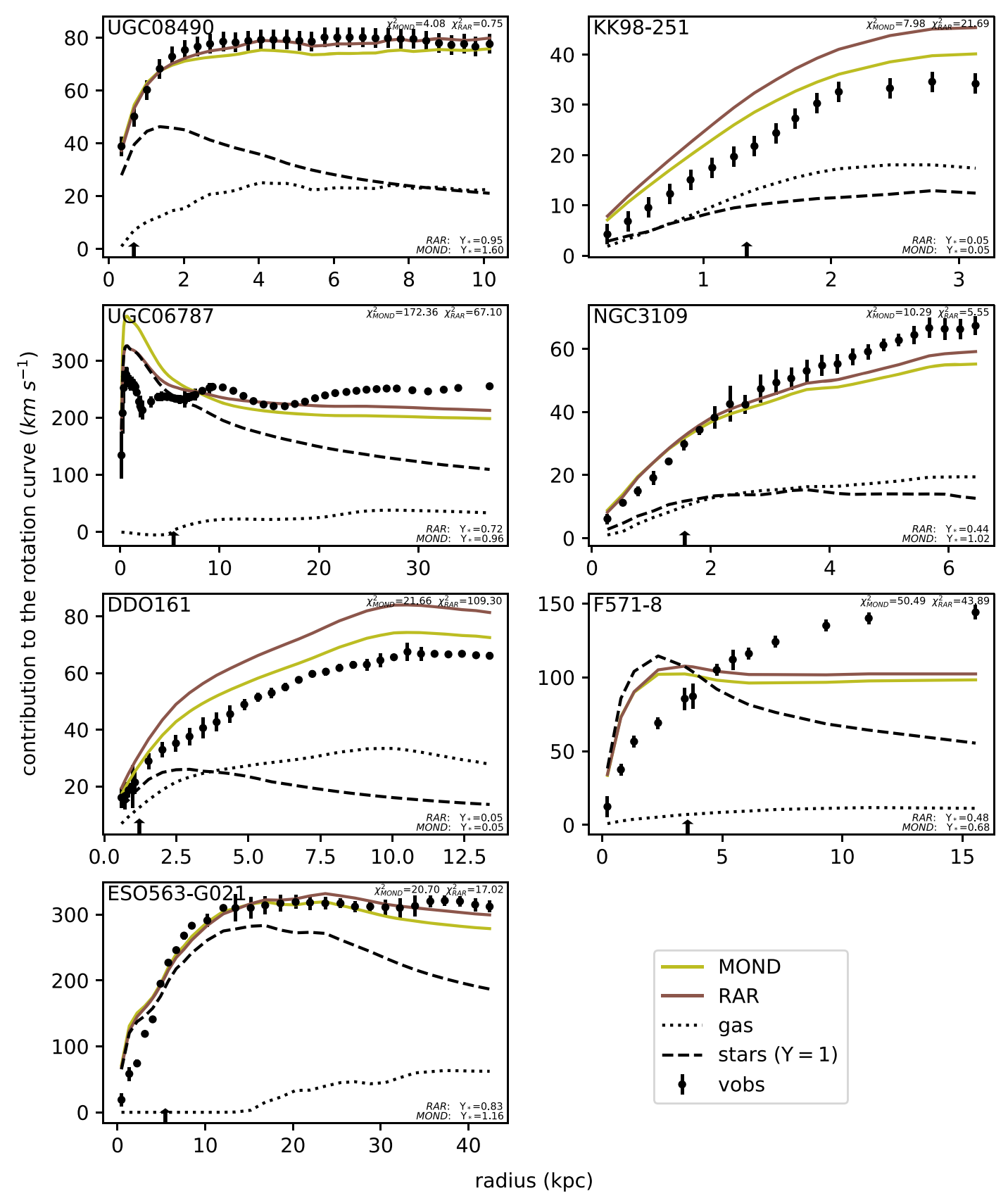


Figure 16. Rotation curve fits of the MOND models. The green line is the total velocity derived from the historic MOND, and the brown line is the total velocity from the RAR model.

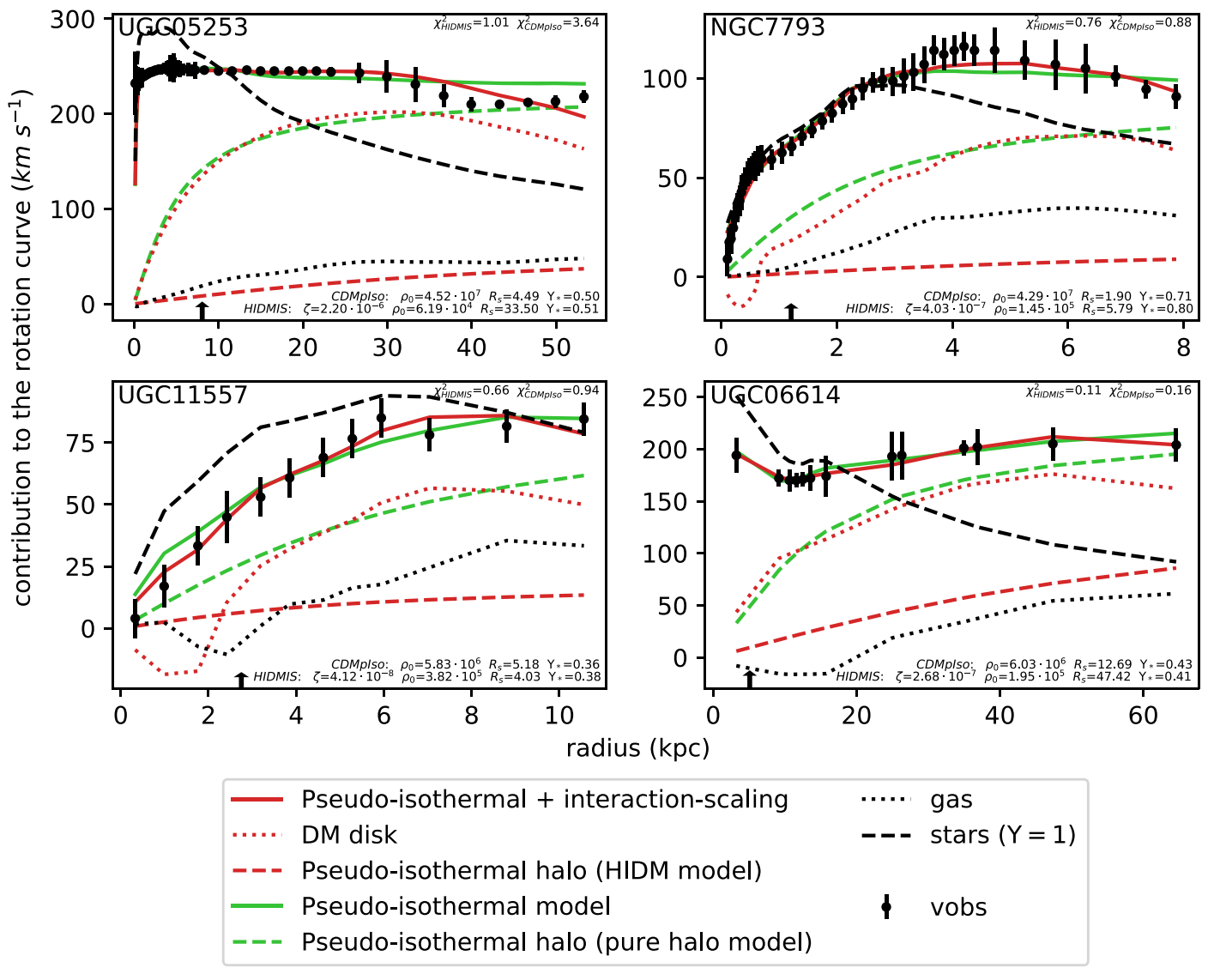


Figure 17. The HIDM-IS (red) and pIso (green) fits for the four galaxies that have a DM disk more massive than the DM halo. The contribution of the stars is displayed for $\Upsilon_* = 1 M_{\odot}/L_{\odot}$; the best-fit values of Υ_* , χ^2 , and other fit parameters for each galaxy are given in the panel legends.

best fit; in all cases, the stellar contribution is shown for $\Upsilon_*=1$ M_{\odot}/L_{\odot} . Figures 12 and 13 display the fits of the four models with DM exclusively in halos: NFW, pIso, Einasto, and SIDM. Figure 14 displays the fits of the two HIDM models having a pIso halo in addition to a DM disk derived in two different ways from the measured gas distribution, as detailed in Appendices A.3 and A.4. Figure 15 shows the fits with the total baryon scaling model, and Figure 16 shows the MOND and RAR model results. Finally, Figure 17 shows the rotation curve fits for HIDM-IS for four galaxies in which the DM disk is more massive than the DM halo.

The seven galaxies we adopt for illustrative purposes are as follows.

 The rotation curve of UGC 06787 contains oscillations that the baryonic components alone cannot explain. As these oscillations come from the gas contribution, the model that best fits this galaxy is the HIDM-GS model. The very peaked inner star contribution and the rotation curve oscillations make the SIDM fits particularly bad.

- The gas contribution is too small to explain the oscillations in an SIDM context.
- Galaxy NGC 3109 is very well fitted by the pIso halo alone, which gives results almost equal to the HIDM-GS model. This is due to the fact that the contribution of the DM disk to the rotation curve is negligible.
- 3. The MOND model gives a poor description of the small galaxy KK 98-251 because v_{tot} is increasing at a large radius while the baryonic components are flat.
- 4. Galaxy UGC 08490 has a characteristically flat rotation curve and slowly increasing inner curve for which MOND models give particularly good results. The RAR MOND model (Equation (A23)) performs even better here. The smooth core and flat rotation curve make the SIDM model work particularly well, with $r_1 = 8.4$ kpc.
- 5. The MOND model fails to explain the rotation curve of F571-8. Indeed, the lack of gas contribution at a large radius does not allow one to explain the slowly increasing pattern of the rotation curve. Thus, the models that add a halo are particularly efficient compared to MOND. In

- addition, we note a very strong contribution due to the DM disk in the HIDM-GS model.
- 6. Galaxy ESO 563-G021 is relatively well fitted by the total baryon scaling model. Here the optimal fit for the HIDM-GS model does not involve a DM disk. This example is typical of a subset of about 70 galaxies with few or no DM disks ($\theta < 10^{-4}$).
- 7. The pIso halo alone gives a good fit for DDO 161. Here the RAR MOND model gives worse results than the first MOND model.

ORCID iDs

Nicolas Loizeau https://orcid.org/0000-0001-5117-2732 Glennys R. Farrar https://orcid.org/0000-0003-2417-5975

References

```
Blumenthal, G. R., Faber, S. M., Primack, J. R., & Rees, M. J. 1984, Natur,
Bullock, J. S., & Boylan-Kolchin, M. 2017, ARA&A, 55, 343
Burkert, A. 1995, 447, 447, L25
Casertano, S. 1983, MNRAS, 203, 735
Chan, T. K., Kereš, D., Oñorbe, J., et al. 2015, MNRAS, 454, 2981
Chemin, L., de Blok, W. J. G., & Mamon, G. A. 2011, AJ, 142, 109
Durkalec, A., et al. 2015, A&A, 576, L7
Dvorkin, C., Blum, K., & Kamionkowski, M. 2014, PhRvD, 89, 023519
Einasto, J. 1965, TrAlm, 5, 87
Farrar, G. R. 2017a, arXiv:1708.08951
Farrar, G. R. 2017b, ICRC (Busan), 301, 929
Farrar, G. R. 2018, arXiv:1805.03723
Farrar, G. R., Wang, Z., & Xu, X. 2020, arXiv:2007.10378
Gentile, G., Salucci, P., Klein, U., Vergani, D., & Kalberla, P. 2004, MNRAS,
   351, 903
Gluscevic, V., & Boddy, K. K. 2018, PhRvL, 121, 081301
```

Hayashi, E., Navarro, J. F., & Springel, V. 2007, MNRAS, 377, 50

```
Hui, L., Ostriker, J. P., Tremaine, S., & Witten, E. 2017, PhRvD, 95, 043541
Jimenez, R., Verde, L., & Oh, S. P. 2003, MNRAS, 339, 243
Kalberla, P. M., & Kerp, J. 2009, ARA&A, 47, 27
Kaplinghat, M., Keeley, R. E., Linden, T., & Yu, H.-B. 2014, PhRvL, 113,
  021302
Kaplinghat, M., Tulin, S., & Yu, H.-B. 2016, PhRvL, 116, 041302
Katz, H., Lelli, F., McGaugh, S. S., et al. 2016, MNRAS, 466, 1648
Lelli, F., McGaugh, S. S., & Schombert, J. M. 2016, AJ, 152, 157
Li, P., Lelli, F., McGaugh, S., & Schombert, J. 2020, ApJS, 247, 31
Loizeau, N., & Farrar, G. R. 2021, arXiv:2106.14915
Markevitch, M., et al. 2004, ApJ, 606, 819
McGaugh, S. S., Lelli, F., & Schombert, J. M. 2016, PhRvL, 117,
  201101
McGaugh, S. S., & Schombert, J. M. 2014, AJ, 148, 77
Meidt, S. E., Schinnerer, E., van de Ven, G., et al. 2014, ApJ, 788, 144
Milgrom, M. 1983, ApJ, 270, 365
Navarro, J. F., Eke, V. R., & Frenk, C. S. 1996, MNRAS, 283, L72
Navarro, J. F., Frenk, C. S., & White, S. D. M. 1996, ApJ, 462, 563
Navarro, J. F., Frenk, C. S., & White, S. D. M. 1997, ApJ, 490, 493
Navarro, J. F., Hayashi, E., Power, C., et al. 2004, MNRAS, 349, 1039
Noordermeer, E. 2006, PhD thesis, Groningen: Rijksuniversiteit
Pontzen, A., & Governato, F. 2012, MNRAS, 421, 3464
Ren, T., Kwa, A., Kaplinghat, M., & Yu, H.-B. 2019, PhRvX, 9, 031020
Rubin, V. C., Ford, W. K. J., & Thonnard, N. 1980, ApJ, 238, 471
Santos-Santos, I. M. E., Navarro, J. F., Robertson, A., et al. 2020, MNRAS,
  495, 58
Scarpa, R. 2006, in AIP Conf. Proc, 822, 1st Crisis in Cosmology Conf.
  (Melville, NY: AIP), 253
Schombert, J., & McGaugh, S. 2014, PASA, 31, e036
Schombert, J., McGaugh, S., & Lelli, F. 2018, MNRAS, 483, 1496
Schutz, K., Lin, T., Safdi, B. R., & Wu, C.-L. 2018, PhRvL, 121, 081101
Spergel, D. N., & Steinhardt, P. J. 2000, PhRvL, 84, 3760
Swaters, R. A., Bershady, M. A., Martinsson, T. P. K., et al. 2014, ApJL,
Swaters, R. A., Sancisi, R., van der Hulst, J. M., & van Albada, T. S. 2012,
   MNRAS, 425, 2299
van den Bosch, F. C., & Swaters, R. A. 2001, MNRAS, 325, 1017
Wadekar, D., & Farrar, G. R. 2021, PhRvD, 103, 123028
Xu, W. L., Dvorkin, C., & Chael, A. 2018, PhRvD, 97, 103530
Xu, X., & Farrar, G. R. 2021, arXiv:2101.00142
```